Mountain, G.S., Miller, K.G., Blum, P., Poag, C.W., and Twichell, D.C. (Eds.), 1996
Proceedings of the Ocean Drilling Program, Scientific Results, Vol. 150

10. SEQUENCE-STRATIGRAPHIC SIGNIFICANCE OF GLAUCONY-RICH LITHOFACIES AT SITE 903[1]

S.R. McCracken,[2] J. Compton,[3] and K. Hicks[3]

ABSTRACT

Extensive glaucony-rich sediment was recovered at Site 903 of Ocean Drilling Program Leg 150, drilled on the upper slope of the New Jersey Margin. Sedimentological, petrological, and geochemical analyses were undertaken on six glaucony-rich intervals (G1–G6) of late Oligocene, Miocene, and middle Pliocene–early Pleistocene age. Three characteristics must be considered in the sequence-stratigraphic interpretation of glaucony-rich sediment on the slope: (1) the degree of reworking undergone by the glaucony prior to its final deposition; (2) the relative abundances of terrigenous and biogenic material in the glaucony-rich unit; and (3) the sedimentological and diagenetic characteristics of the lower boundary of the glaucony-rich unit. In contrast to typical shelf settings, the glaucony-rich sediments observed in Site 903 were deposited during three different stages within the depositional sequence: during sediment starvation of the basin during maximum transgression (G1 and G2: late Oligocene to early Miocene), during early highstand (G3, G4, and G5: middle to late Miocene), and during lowstand (G6: middle Pliocene–early Pleistocene).

INTRODUCTION

A major objective of Ocean Drilling Program (ODP) Leg 150 was "to sample boundaries of depositional sequences that are seismically imaged on the shelf but which can be dated with greater precision on the slope" (Miller and Mountain, 1994, p. 19). Site 903 was the most landward site drilled on Leg 150, drilled 4.1 km downslope from the modern shelf edge in ~445 m of water (Fig. 1). This site provided the best opportunity to correlate depositional events with seismic reflectors that can be traced to shelfal sequence boundaries. Unfortunately, the diagenetic removal of calcareous microfossils from the middle to upper Miocene strata drilled at Site 903 greatly complicated the sequence stratigraphic interpretation of this section. The absence of detailed biostratigraphic information not only hampered the dating of sequence boundaries, but also made the initial identification of sequence boundaries difficult.

The Eocene to Pleistocene strata drilled at Site 903 (Fig. 2) were deposited on the upper slope, a depositional setting that has largely been ignored by sequence stratigraphers. The features that define sequence boundaries on the slope are, by definition, different from those that characterize sequence boundaries as originally defined by Vail et al. (1977). Sequence boundaries are the result of subaerial erosion and nondeposition due to relative sea-level fall (Van Wagoner et al., 1988) and therefore the expression of sequence boundaries or correlative surfaces on the slope may be as periods of increased clastic sedimentation rather than a single, recognizable surface (Haq, 1991). Nevertheless, the characteristics of sequence boundaries on the slope, and the sequences they enclose, reflect the processes operating in the laterally equivalent, shelfal settings.

Identification of sequence boundaries in the middle to upper Miocene section at Site 903 relied upon identification of unconformities and terrigenous-rich units. Two mechanisms have been identified in the literature for the development of unconformities in deep-sea settings such as the slope: (1) large relative sea-level falls associated with second-order sequence boundaries can lead to the development of significant erosional boundaries overlain by reworked terrigenous sediment (Poag and Ward, 1987), and (2) sediment starvation during flooding of the shelf can lead to development of nondepositional hiatuses overlain by authigenic minerals such as glauconite and phosphate (Haq, 1991). The middle to upper Miocene section observed at Site 903 is characterized by common erosional surfaces overlain by both terrigenous-rich sediment and glaucony-rich sediment (Fig. 2). Identification of the mechanisms by which these surfaces and their associated terrigenous- and glaucony-rich sediment have formed is critical for the sequence-stratigraphic analysis of this section.

The term "glaucony" warrants some comment. The term glaucony (Millot, 1970) was used by Odin and Matter (1981) to distinguish the marine facies characterized by green grains from the individual mineral components (green smectite, mixed-layer glauconite and smec-

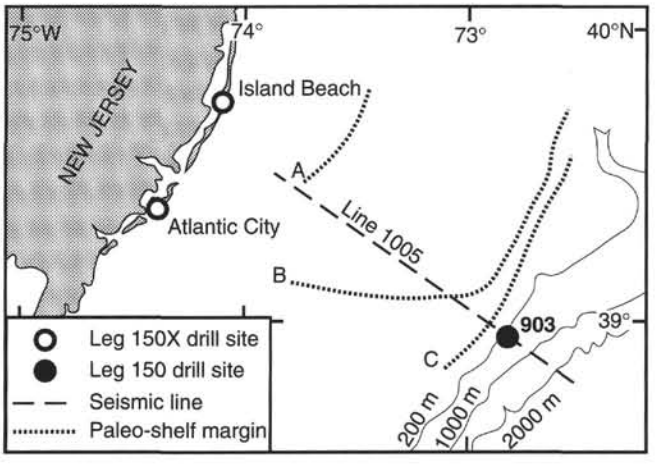

Figure 1. Location of Site 903. The approximate positions of the early Miocene (A), middle Miocene (B), and late Miocene (C) shelf margins are shown in relation to Site 903 (after Greenlee and Moore, 1988).

[1]Mountain, G.S., Miller, K.G., Blum, P., Poag, C.W., and Twichell, D.C. (Eds.), 1996. *Proc. ODP, Sci. Results,* 150: College Station, TX (Ocean Drilling Program).
[2]Department of Geology and Geophysics, University of Western Australia, Nedlands, 6907, Western Australia, Australia. smccrack@geol.uwa.edu.au
[3]Department of Marine Science, University of South Florida, 140 Seventh Avenue South, St. Petersburg, FL 33701-5016, U.S.A.

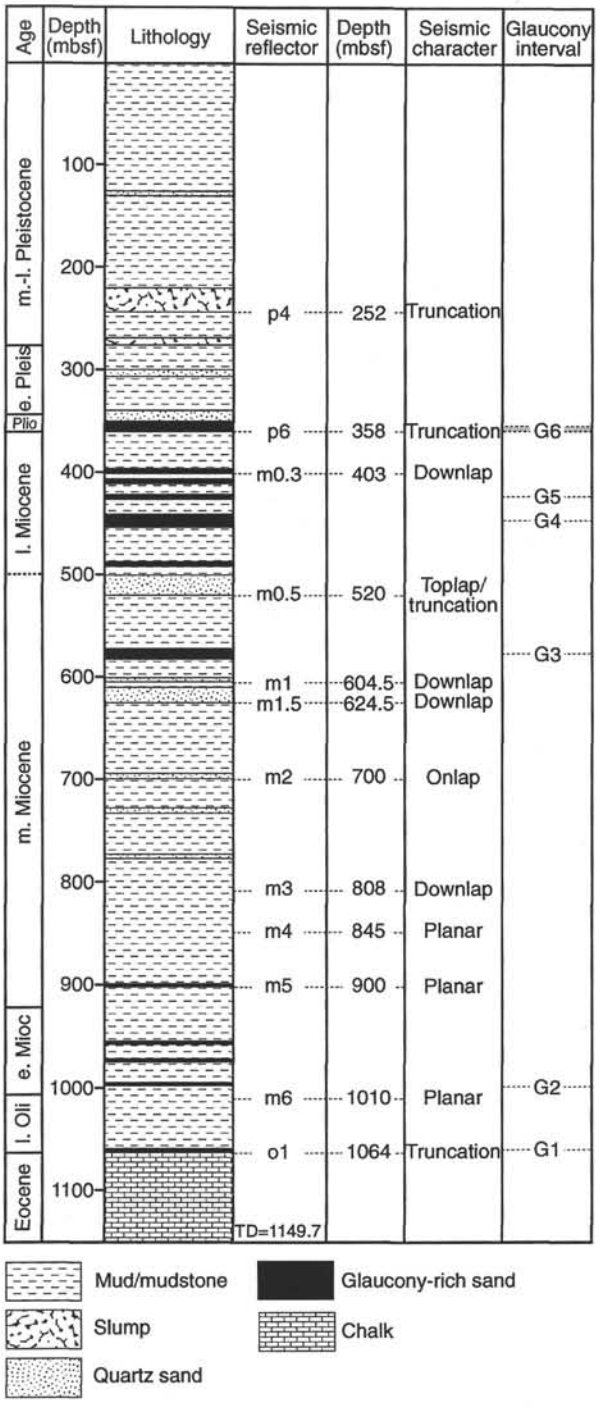

Figure 2. Composite stratigraphic column for Site 903 incorporating data from Holes 903A, 903C, and 903D. The lithologic correlations of the seismic reflectors drilled at Site 903 (after Shipboard Scientific Party, 1994) and the positions of the glaucony intervals sampled for this study are shown.

tite, and glauconite) of this facies. Confusingly, this term was also used by these authors for individual green grains. In this paper, unless the mineralogy of the grains is being discussed, the term glaucony will be used when referring to green grains. "Glauconitization" is the process of the replacement of microfossils, biogenic material, or fecal pellets at or near the sediment/water interface by glaucony (Odin and Matter, 1981).

A significant problem recognized by the shipboard scientists was the inability to identify confidently whether the abundant glaucony present in the middle to upper Miocene section of Site 903 had formed in situ or had been transported from precipitation sites on the shelf. As this has significant implications for the understanding of the sequence stratigraphy of this section, three glaucony-rich units were chosen from the middle to upper Miocene section of Site 903 for more detailed study (Fig. 2: intervals G3, G4, and G5). Units were also chosen from the upper Oligocene–lower Miocene (Fig. 2: G1 and G2) and middle Pliocene–lower Pleistocene (Fig. 2: G6) of Site 903.

SEQUENCE STRATIGRAPHY OF SITE 903

The Eocene to Pleistocene section drilled at Site 903 records the progradation of the Neogene siliciclastically dominated depositional sequences across a broad Paleocene pelagic carbonate shelf. Slow subsidence of the margin combined with a dramatic increase in the terrigenous sediment supply resulted in the rapid, easterly migration of the shelf margin in the Miocene (Fig. 1; Greenlee and Moore, 1988; Greenlee et al., 1992). This progradation of the Miocene clinoformal packages across the shelf is reflected in the apparent increase upsection in sedimentation rates (Shipboard Scientific Party, 1994) and the increased significance of coarse terrigenous sediment and terrestrial organic matter in the middle to upper Miocene strata observed at Site 903.

Previous studies of the Neogene depositional sequences of the New Jersey Margin (Greenlee et al., 1992) have suggested that the geometric and lithostratigraphic expression of these sequences is different from the idealized sequence stratigraphic model (Vail et al., 1977; Van Wagoner et al., 1988). The most significant variation from the model in the context of the present study is the apparent absence of the transgressive system tract in the Neogene depositional sequences of the New Jersey Margin (Greenlee et al., 1992). This is suggested to be the result of the low subsidence rates of this margin and the slow, second-order eustatic fall observed during the Neogene. The presence of thick, glaucony-rich units in the Miocene drilled at Site 903, a sediment type generally associated with the transgressive system tract and associated condensed sections (Loutit et al., 1988) appears to contradict this assertion. The origin of this glaucony is therefore critical in understanding the sequence-stratigraphic architecture of this margin.

METHODS

Samples for this study were selected from directly below, within, and directly above six glaucony-rich units at Site 903 (Fig. 2). Carbonate nodules present below the lower boundaries of these units were sampled for stable isotope analysis. To avoid confusion in discussing the various glaucony-rich intervals described in this study, the six intervals were labelled as defined in Table 1.

The samples for grain-size analysis and grain-type modal analysis were dried and weighed. Each sample was then disaggregated by boiling for 1 hr in a Calgon and detergent solution and washed through 2-mm, 150-μm, and 63-μm sieves. The three coarser fractions were dried and weighed separately to determine their weight percent (Table 2). The proportion of the sample represented by the <63-μm fraction (lost during sieving) was calculated from the total weight determined prior to sieving (Table 2). Difficulties were encountered in processing the samples from intervals G1 and G2 due to the presence of diagenetic cements. Processing in hydrogen peroxide and kerosene failed to totally disaggregate the samples. Therefore, grain-size analysis of these intervals was abandoned and the shipboard smear-slide data (Shipboard Scientific Party, 1994) were used in place of grain-size data. Partially disaggregated samples from in-

Table 1. Intervals containing glaucony-rich units investigated for this study.

Glaucony interval	Interval		Age
	Top	Base	
G1	150-903C-51R-6, 110 cm (1061.97 mbsf)	52R-1, 20 cm (1064.3 mbsf)	late Eocene to late Oligocene
G2	150-903D-21R-4, 40 cm (999.87 mbsf)	21R-4, 120 cm (1000.67 mbsf)	early Miocene
G3	150-903A-64X-2, 5 cm (579.05 mbsf)	64X-4, 85 cm (582.85 mbsf)	middle Miocene
G4	150-903A-49X-5, 130 cm (440 mbsf)	51X-2, 110 cm (455 mbsf)	late Miocene
G5	150-903A-47X-6, 100 cm (422.2 mbsf)	48X-5, 20 cm (429.5 mbsf)	late Miocene
G6	150-903A-39X-1, 120 cm (337.6 mbsf)	41X-3, 25 cm (358.95 mbsf)	late Miocene to early Pleistocene

tervals G1 and G2 were mounted in epoxy resin and thin sectioned to enable petrographical analysis of the glaucony and estimation of the abundance of terrigenous and biogenic material in these samples. Thin sections of grain mounts were also prepared for intervals G3, G4, G5, and G6 for petrographic analysis of the glaucony and terrigenous fraction. The disaggregated samples were point counted (N = 500) to determine the percentages of the various grain types (Table 2).

Carbon and oxygen isotope analysis of carbonate nodules and beds (Table 3) was undertaken at the University of Tasmania. Samples of nodules were finely crushed and septarian vein material was removed using a dental drill. Samples of 100 to 200 mg were dissolved in 100% phosphoric acid in a water bath at 50°C for 24 to 48 hr using the method of McCrea (1950). The isotopic compositions of carbon and oxygen in the extracted CO_2 was obtained from a VG SIRA series II stable isotope mass spectrometer. Corrections according to Craig (1957) were applied to the values obtained. A further correction of 1‰ was added to the oxygen value to compensate for the higher reaction temperature (+0.04‰ per degree Centigrade above 25°C). The dolomite sample from interval G2 (Fig. 6; Sample 150-903D-21R-8, 46–49 cm) was analyzed at the University of South Florida (see Hicks et al., this volume, for methods). Polished thin sections of the nodules and the dolostone beds were examined using a Nuclide ELM 2A luminoscope at the University of Melbourne. Photography of the luminescent images required 1600 ASA film because of the very dull luminescence emitted by these samples.

The presence of glauconite in the samples was confirmed by X-ray diffraction (XRD; Fig. 3) using Cu Ka radiation on a Phillips PW1700 instrument at the University of Western Australia. The bulk samples were washed with deionized water through a 63-µm sieve to separate the sand fraction from the silt- and clay-sized fractions. The sand-sized fraction was dried at 60°C overnight. Whole and broken glaucony grains >300 µm in size were examined on an ISI-DS130 scanning electron microscope (SEM) at University of South Florida.

SEDIMENTOLOGY OF GLAUCONY-RICH UNITS

Upper Oligocene to Lower Miocene

The upper Oligocene to lowermost Miocene strata at Site 903 are characterized by brown-gray nannofossil silty claystones with rare glauconitic beds, dolostone beds, and dolomite nodules, and an absence of siderite nodules and terrigenous plant material. Tentative sedimentation rate calculations for the upper Oligocene at Site 903 suggest sedimentation rates of approximately 0.5 cm/1000 yr (Shipboard Scientific Party, 1994), which is significantly slower than during the middle to late Miocene. The late Oligocene shelf margin was approximately 140 km west of Site 903, in a similar location to the present-day shoreline (Greenlee and Moore, 1988). The upper Oligocene section represents the initial influx of terrigenous material that extended into the slope basin offshore New Jersey as far as Site 903. In the earlymost Miocene, the shelf edge migrated 50 km to the east (Fig. 1; Greenlee and Moore, 1988). This basinal shift had no perceptible effect on sedimentation at Site 903. The two glaucony-rich intervals studied in this succession both appear to represent erosional/nondepositional surfaces.

Glaucony-rich interval G1 (Sections 150-903C-51R-6, 110 cm, to 52R-1, 20 cm; 1061.97–1064.3 mbsf) consists of an upper Oligocene, 2-m-thick, variably cemented, highly bioturbated, glaucony-rich unit, which unconformably overlies upper Eocene nannofossil chalk (Figs. 4, 5). This erosional unconformity is correlated to seismic reflector o1 (Fig. 2). The lower boundary is a sharp, eroded/burrowed surface, quartz is a minor component of the sediment, and the glaucony content decreases uphole to a gradational upper boundary. Abundant radiolarians, foraminifers, and rare fish fragments are present in this unit. The dark green, rounded to well-rounded glaucony grains have well-developed shrinkage cracks (Pl. 1, Figs. 1 and 2). The grains typically contain preserved relic radiolarians and show only minor evidence of reworking. Minor pyrite is present within the shrinkage cracks of grains and the cracks are commonly overgrown by light green glaucony (Pl. 1, Fig. 1). The calcite-cemented intervals of the glaucony sands contain common compaction features such as flattened grains indicating that cementation and lithification postdate significant compaction of the sediment (Pl. 1, Fig. 3). The top 15 cm of the underlying Eocene chalk is partially to totally replaced by 30- to 50-µm rhombic dolomite crystals (Pl. 2, Figs. 1 and 2; see Fig. 4 and Table 3 for carbon and oxygen isotopic values). Iron-poor dolomite rhombs precipitated within foraminifer tests are overgrown by pore-filling, Fe-rich dolomite. The Fe-poor dolomite rhombs display a complex cathodoluminescent zoning (Pl. 2, Fig. 2).

Glaucony-rich interval G2 (Sections 150-903D-21R-4, 40 cm, to 21R-4, 120 cm; 999.87–1000.67 mbsf) is present 9.5 m above a zone of poor core recovery considered to represent a cemented sand bed associated with the m6 reflector (Shipboard Scientific Party, 1994). M6, as recognized on Leg 150, correlates to an unconformity between the upper Oligocene (NP25) and the lower Miocene (NN2) (Fig. 2). The base of the glaucony-rich unit (within glaucony-rich interval G2) at 1000.54 mbsf is associated with a stratigraphic gap of 2 m.y. indicated by strontium dating (Miller et al., this volume). The glaucony-rich unit has a sharp, eroded/burrowed lower boundary, a transitional upper boundary and consists of highly bioturbated, clayey siltstone with abundant sand-sized glaucony and minor quartz (Fig. 6). *Planolites* infilled with glaucony-rich sediment are present up to 30 cm below the lower boundary of the bed. The glaucony grains can be separated into three populations: (1) dark green, spherical to prolate grains with well-developed shrinkage cracks; (2) radiolarians partially replaced by glaucony; and (3) variably rounded, fractured grains (Pl. 1, Figs. 4 and 5). Radiolarians are abundant in the unit and display progressive replacement by glaucony from glaucony-free to glaucony grains with ghosts of radiolarians preserved within them (Pl. 1, Figs. 4 and 5). Pyrite is common along fractures in the glaucony grains. Dolostone beds are present 4 and 5 m below

Table 2. Grain-size data (weight percent) and grain-type modal percentages for the middle Pliocene to lower Pleistocene and Miocene intervals.

Interval	Core, section, interval (cm)	Depth (mbsf)	Grain-size fraction (wt%)			Grain type															
						Modal %: >150-µm fraction								Modal %: <150-µm fraction							
			<63 µm	>63 µm	>150 µm	>2 mm	Q	G	F	R	M	H	P	Q	G	F	R	M	H		
	150-903A-																				
G6	40X-4, 77–79	351.27	28.0	12.6	59.3	0.1	64.0	35.8	0.2	0.0	0.0	0.0	0.0	23.2	75.8	0.0	0.0	0.8	0.2		
	41X-1, 65–67	356.35	34.8	16.0	48.7	0.5	48.4	51.4	0.0	0.0	0.2	0.0	0.0	18.8	80.2	0.4	0.0	0.0	0.6		
G5	48X-1, 76–78	424.06	67.7	7.5	24.3	0.4	95.8	3.6	0.0	0.0	0.4	0.2	0.0	91.6	5.4	0.2	0.0	0.2	2.6		
	48X-2, 77–79	425.57	57.6	32.0	10.4	0.0	88.2	7.6	0.0	0.0	3.0	0.0	1.2	72.4	23.2	0.0	0.0	2.6	1.8		
	48X-4, 75–77	428.55	53.8	32.2	14.1	0.0	66.6	32.6	0.0	0.0	0.8	0.0	0.0	77.6	19.4	0.0	0.0	2.4	0.6		
	48X-5, 75–77	430.05	93.4	2.2	4.4	0.0	37.5	11.0	35.5	1.0	15.0	0.0	0.0	63.6	9.62	0.0	4.0	2.8	0.0		
G4	49X-5, 77–79	439.77	97.2	1.6	1.2	0.0	40.8	50.6	5.6	2.4	0.6	0.0	0.0	62.2	29.4	1.6	6.2	0.4	0.2		
	49X-6, 77–79	441.27	40.2	25.0	34.8	0.0	47.6	52.4	0.0	0.0	0.0	0.0	0.0	14.8	84.8	0.0	0.0	0.0	0.4		
	50X-1, 30–32	443	51.2	20.7	27.9	0.3	53.2	46.8	0.0	0.0	0.0	0.0	0.0	29.0	70.4	0.2	0.0	0.0	0.4		
	50X-5, 30–32	449	37.6	19.2	43.2	0.0	84.4	15.0	0.0	0.0	0.4	0.2	0.0	46.2	53.4	0.2	0.0	0.0	0.2		
	51X-1, 30–32	452.5	55.5	24.2	20.3	0.0	72.6	27.0	0.0	0.4	0.0	0.0	0.0	53.8	45.6	0.0	0.0	0.0	0.6		
	51X-2, 10–12	453.8	54.6	19.8	25.6	0.0	81.2	18.6	0.0	0.0	0.2	0.0	0.0	46.2	52.6	0.0	0.0	0.6	0.6		
	51X-2, 76–78	454.46	49.0	23.8	27.3	0.0	90.4	9.2	0.2	0.0	0.2	0.0	0.0	67.4	31.6	0.0	0.4	0.2	0.4		
	51X-3, 27–29	455.47	90.2	8.8	1.1	0.0	39.6	6.0	0.8	1.0	35.8	0.0	16.8	84.4	3.8	0.4	1.2	9.8	0.4		
G3	64X-2, 115–117	580.15	95.0	4.2	0.8	0.0	56.4	14.0	0.6	1.0	28.0	0.0	0.0	59.4	10.2	0.0	12.6	17.4	0.4		
	64X-3, 75–77	581.25	66.7	11.7	21.6	0.0	72.4	26.6	0.0	0.0	1.0	0.0	0.0	70.8	23.6	0.2	1.2	2.4	1.8		
	64X-4, 20–22	582.2	76.1	11.8	12.2	0.0	58.2	40.8	0.0	0.0	1.0	0.0	0.0	61.8	31.2	0.0	2.2	3.8	1.0		
	64X-4, 69–71	582.69	46.5	9.7	43.7	0.1	72.4	26.8	0.0	0.0	0.6	0.2	0.0	28.0	68.6	0.0	0.8	1.4	1.2		
	64X-4, 105–107	583.36	97.0	1.1	1.9	0.0	83.2	14.6	0.8	0.4	1.0	0.0	0.0	52.4	10.6	0.0	22.0	13.6	1.4		

Notes: Q = quartz, G = glaucony, F = foraminifers, R = radiolarians, M = mica, H = heavy minerals, P = plant material.

the lower boundary of the glaucony-rich bed. The dolostones consist of bioturbated silty claystone replaced by 30- to 50-µm dolomite crystals in an idiotopic fabric (Pl. 1, Fig. 6; see Fig. 6 and Table 3 for carbon and oxygen isotopic values). The precipitation of the dolomite post-dates pyritization of the glaucony and the dolomite crystals display zoning from Fe-poor cores to Fe-rich rims.

Middle to Upper Miocene

During the late middle to early late Miocene, the shelf margin was approximately 10 km landward of Site 903 (Fig. 1; Greenlee and Moore, 1988). Type 1 sequence boundaries that developed during this period on the shelf (m1.5, m1, and m0.5) are recognized at Site 903 by the presence of thick sand units dominated by terrigenous material (Fig. 2). The sequence boundaries m0.3 and m0.5 enclose the problematic latest middle to upper Miocene glaucony-rich succession. Intervals G4 and G5 are part of this succession. The succession bounded by m0.5 and m1 is, in comparison, relatively simple, with only one glaucony-rich interval (G3) present within it.

Glaucony-rich interval G3 is present 20 m from the base of the succession bounded by m0.5 and m1 (Fig. 2). G3 consists of two glaucony-rich beds separated by a 130-cm-thick interval of clayey silt. The upper bed is 50 cm thick and the lower bed is 175 cm thick (Fig. 7). Both beds have sharp, burrowed bases with glaucony sand-filled *Planolites* extending 20 cm below the lower contact. The lower bed (Sections 150-903A-64X-3, 50 cm, to 64X-4, 75 cm; 581.0–582.75 mbsf) was selected for detailed study owing to the presence of a siderite nodule 60 cm below its lower boundary. Grain-size analysis of four samples taken from the glaucony-rich bed and the overlying clayey silt unit suggests the presence of two fining-upward zones, one in the glaucony-rich bed and one within the clay-rich bed (Fig. 7). Glaucony decreases in abundance upcore through the bed. Radiolarians are abundant directly below the lower contact and directly below the lower contact of the overlying glaucony-rich bed. Rare radiolarians and foraminifers were observed in the lower glaucony-rich bed. A poorly cemented nodule of intergrown siderite and calcite is present 60 cm below the lower contact of the lower glaucony-rich bed. The nodule is a buff to pale yellow color, with a diffuse outer boundary and no observable internal structure (see Fig. 7 and Table 3 for carbon and oxygen isotopic values). This nodule is morphologically and isotopically similar to siderite nodules common throughout the middle Miocene section at Site 903 (Hicks et al., this volume).

The two intervals (G4 and G5) selected from the succession between m0.3 and m0.5 (Fig. 2) are very rich in glaucony and contain abundant terrigenous material. Interval G4 (Sections 150-903A-49X-5, 130 cm, to 51X-2, 110 cm; 440–455 mbsf) is a single, highly bioturbated, glaucony-rich unit (Fig. 8). The upper interval, G5 (Sections 150-903A-47X-6, 100 cm, to 48X-5, 20 cm; 422.2–429.5 mbsf), consists of two fining-upward, glaucony-rich beds, each overlying sharp, burrowed boundaries (Fig. 9).

Glaucony-rich interval G4 is highly bioturbated, contains abundant coarse quartz sand, does not appear to be graded, and has gradational upper and lower boundaries with calcite nodules present below it (Fig. 8). The glaucony grains are dark green to yellowish-green in color, variably broken and rounded, commonly pyritized and rarely showing well-preserved radial fractures (Pl. 3, Fig. 1). The glaucony increases in abundance upsection. No microfossils were observed directly below, or within, the glaucony-rich unit. Radiolarians and foraminifers were common in Sample 150-903A-49X-5, 77–79 cm (439.77 mbsf), taken from directly above the unit. Organic material was common in a sample taken directly below the unit. The gradational nature of the lower boundary is due to extensive bioturbation and mixing of glaucony-rich sediment into the underlying silty clay. The calcite nodules developed below the lower boundary are small (5 to 20 mm) and in the case of the upper nodule, contain septarian veins

Table 3. Stable isotope data for diagenetic carbonates associated with the glaucony-rich intervals.

Interval	Core, section, interval (cm)	Depth (mbsf)	Mineralogy	Sample type	$\delta^{13}C$ ‰ (PDB)	$\delta^{18}O$ ‰ (PDB)
150-903A-						
G6	41X-1, 89–94	356.63	Calcite	Reworked nodule	−21.63	4.30
G5	48X-5, 20–22	429.5	Calcite	Nodule	−16.72	4.01
	48X-5, 95–97	430.25	Calcite + siderite	Nodule	−18.72	4.27
G4	51X-3, 116–118	456.37	Calcite	Nodule	−18.50	3.77
	51X-3, 116–118	456.37	Calcite	Vein	−7.83	3.32
G3	64X-4, 136–138	583.36	Calcite + siderite	Nodule	−0.92	5.39
150-903C-						
G1	51R-6, 145–147	1062.07	Calcite	Bed	−0.79	−0.09
	51R-7, 125–127	1063.36	Calcite	Bed	−2.78	−0.43
	52R-1, 9–12	1064.25	Dolomite + calcite	Bed	−1.78	−0.88
150-903D-						
G2	21R-8, 46–49	1005.92	Dolomite	Bed	−2.18	−0.61

Notes: Sample 150-903D-21R-8, 46–49 cm, was analyzed at the University of Southern Florida (see Hicks et al., this volume, for methods). All other samples were analyzed at the University of Tasmania; see "Methods" section for the analytical procedure.

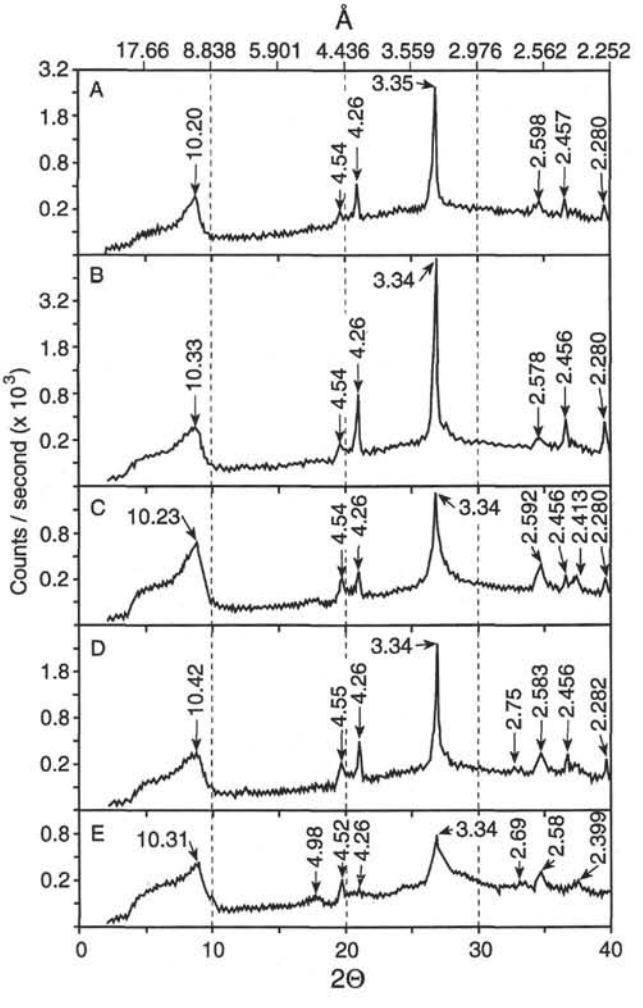

Figure 3. X-ray diffraction patterns of sand-sized glaucony grains with minor quartz (4.26 Å peak). **A.** Sample 150-903A-41X-1, 65–67 cm (356.35 mbsf). **B.** Sample 150-903A-48X-4, 75–77 cm (428.55 mbsf). **C.** Sample 150-903A-49X-6, 77–79 cm (441.27 mbsf). **D.** Sample 150-903A-64X-4, 69–71 cm (582.69 mbsf). **E.** Sample 150-903C-51R-7, 35–37 cm (1063.02 mbsf).

(Pl. 2, Figs. 3 and 4). The body of the nodule consists of iron-poor micrite with common disseminated pyrite. The septarian veins are restricted to the inner parts of the nodule, have sharp boundaries, and are infilled with three phases of iron-poor calcite (Pl. 2, Fig. 4; see Fig. 8 and Table 3 for the carbon and oxygen isotopic values of this nodule).

The two glaucony-rich beds of interval G5 are normally graded and moderately bioturbated (Fig. 9). The lower contacts are sharp and burrowed, with glaucony sand filling the burrows, and the upper contacts are gradational. The limited grain-size analyses undertaken for this study suggest the following trends within the lower glaucony-rich bed of G5: glaucony decreases in abundance upsection, quartz increases in abundance, and the silty clay between the two glaucony-rich beds contains up to 25% medium to coarse quartz sand (Fig. 9). Microfossils (foraminifers and radiolarians) are common in the clayey silt directly below the sharp lower contact, are totally absent throughout the glaucony-rich bed, and were not observed directly above the bed. Plant material is abundant throughout both glaucony-rich beds. The glaucony is petrographically similar to the glaucony in G4 (Pl. 3, Fig. 2). Rare quartz, feldspar, and mica grains are partially replaced by glaucony. *Planolites* is the dominant ichnofossil observed.

A 10-cm-thick, well-cemented calcite nodule is present 10 cm below the sharp boundary of the lower unit of interval G5 (Fig. 9). The glaucony sand-filled *Planolites* stop at the top surface of the nodule and are absent within and below the nodule. The nodule consists of iron-poor micrite and contains pyritized and unaltered foraminifers (see Fig. 9 and Table 3 for the carbon and oxygen isotopic values of this nodule). Poorly cemented nodules of intergrown calcite and siderite are present 95 and 195 cm below the contact. The nodules contain common disseminated pyrite, have diffuse margins, and do not appear to display core to rim chemical zoning (see Fig. 9 and Table 3 for the carbon and oxygen isotopic values of the upper of these nodules).

Middle Pliocene to Lower Pleistocene

Glaucony-rich interval G6 (Sections 150-903A-39X-1, 120 cm, to 41X-3, 25 cm; 337.6–358.95 mbsf) consists of a series of normally graded units with the lowermost unit overlying a sharp erosional contact with upper Miocene clayey silt (Fig. 10). The lower part of this interval appears to be middle to late Pliocene in age, and the upper part early Pleistocene (Shipboard Scientific Party, 1994). Reworked Paleocene and Eocene calcareous nannofossils are present in Core 150-903A-38X, ~2 m above the uppermost graded bed. The erosional boundary at the base of G6 is interpreted as a sequence boundary and is correlated to the p6 seismic reflector (Fig. 2; Shipboard Scientific Party, 1994).

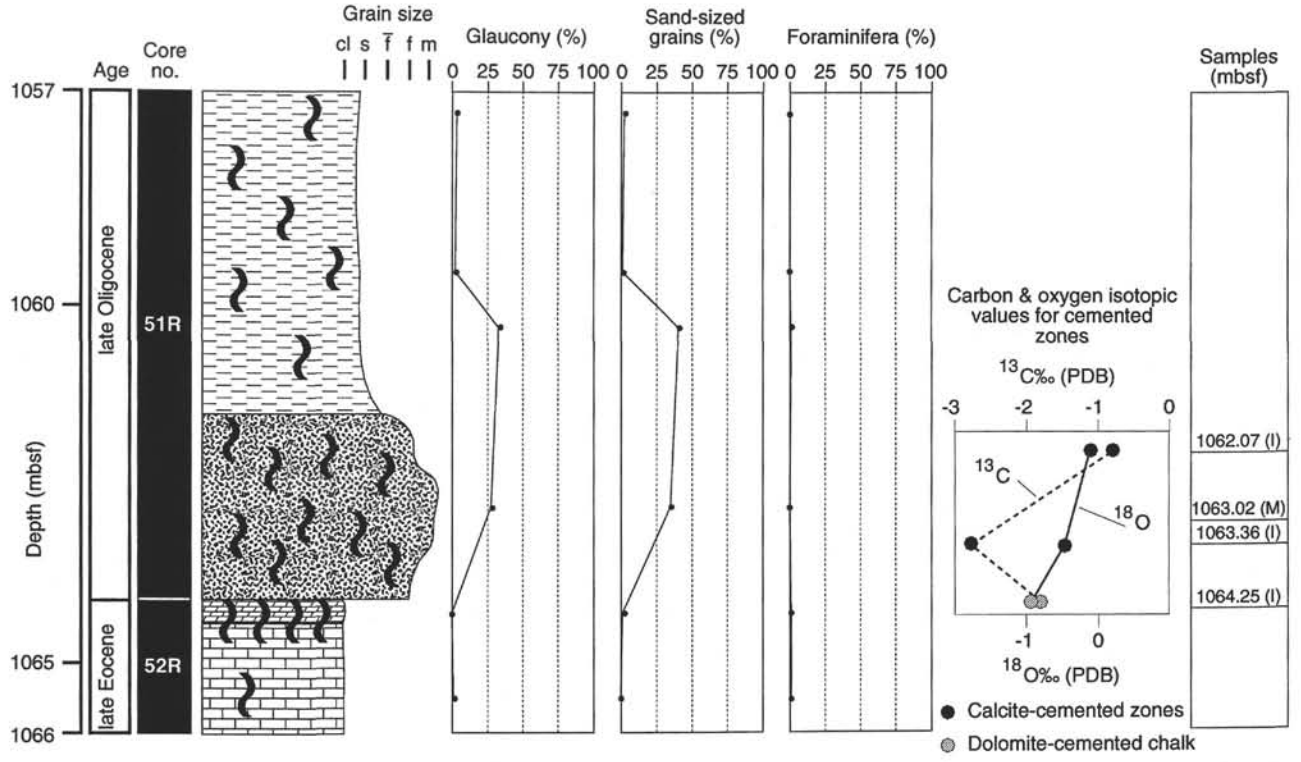

Figure 4. Detailed sedimentological log of glaucony-rich interval G1 (refer to Table 1 for core details). Smear-slide data from Shipboard Scientific Party (1994). See Table 3 for isotopic data. See Figure 5 for the key to symbols used.

The glaucony grains present in the five graded beds are mottled dark to light brownish-green, fractured, variably rounded, and commonly replaced by pyrite (Pl. 3, Fig. 3). Brown glaucony grains, indicative of oxidation and possible exposure, are very rare in this unit. The glaucony-rich graded beds also contain abundant, poorly sorted, variably rounded, fine to very coarse quartz sand (Pl. 3, Fig. 3). Rare quartz grains are partially replaced by glaucony.

A significant feature of these sands is the presence of rounded clasts of calcite-cemented glaucony and quartz sand with common shrinkage features such as calcite-lined fractures and calcite-filled cavities around the grains (Pl. 2, Figs. 5 and 6, and Pl. 3, Fig. 4). These shrinkage features are similar to the shrinkage cracks that characterize septarian nodules (see Fig. 10 and Table 3 for the carbon and oxygen isotopic values of these cements). The iron-poor calcite that fills the shrinkage features overgrows pyrite rims developed on the glaucony grains (Pl. 3, Fig. 4). The glaucony within these carbonate clasts is petrographically similar to the glaucony of G4 and G5 (Pl. 3, Fig. 4). Rare foraminifers are present in these clasts, including specimens of *Globigerinoides* spp. and a single specimen tentatively identified as *Globorotalia menardii.* These foraminifers are consistent with a Miocene age. Strontium isotopic analyses suggest that the diagenetic cements in the clasts were precipitated in the middle Miocene (Hicks et al., this volume). These clasts are interpreted to be nodules reworked from Miocene strata exposed upslope from Site 903.

DISCUSSION

Factors Controlling Glaucony Formation

The mechanism of glauconitization begins close to, or at, the sediment/water interface and is promoted by the presence of granular sediment (Odin and Fullagar, 1988). Glaucony preferentially replaces porous substrates, as crystal growth begins within pore spaces (Odin and Fullagar, 1988) rather than by the alteration of a parent layer silicate (Hower, 1961). Glauconitization proceeds initially by the dissolution of clay precursors and the simultaneous precipitation of glaucony followed by a stage of crystal maturation characterized by ion exchange with the surrounding marine environment (Stille and Clauer, 1994). Glaucony requires a partially reducing environment in which to precipitate, such as the semiconfined microenvironment within microfossil tests and porous fecal pellets (Odin and Matter, 1981) or the reducing environment developed in the oxygen-minimum layer (Jenkyns, 1986). Porous grains that are mobile on the seafloor are more susceptible to glauconitization owing to the constant renewal of the ion supply around the grains. Burial of glaucony grains slows down and finally halts the process of glauconitization as interstitial fluids in sediments are not as enriched in ions as seawater (Odin and Fullagar, 1988). The broad climatic and depth ranges of modern glaucony formation limit its use as a indicator of paleo-depth and climate (see Odin, 1988, for a review of green clay minerals).

The evolution of a glaucony grain is a complex process that depends upon the nature of the initial substrate and the duration of the hiatus at which the glaucony forms. Four phases of glauconitization have been recognized (Fig. 11; Odin and Dodson, 1982). The "nascent" stage represents the infilling of the available pore space in the grain. "Slightly evolved" grains form by the infilling of pore space created by the destruction of the grain. The "evolved" stage involves the preferential recrystallization and growth of the grain center. Expansion of the grain center results in the cracking of the exterior of the grain and commonly leads to fracturing of the grains. In the final "highly evolved" stage, the cracks formed in the previous phase are filled by lighter green glaucony and the surface of the grains becomes smooth. Chemical changes also take place during this morphological evolution of the glaucony grain, with K_2O content increasing from ~2% in nascent grains to >8% in highly evolved grains. Odin and Dodson (1982) estimated that the evolution of a highly evolved grain

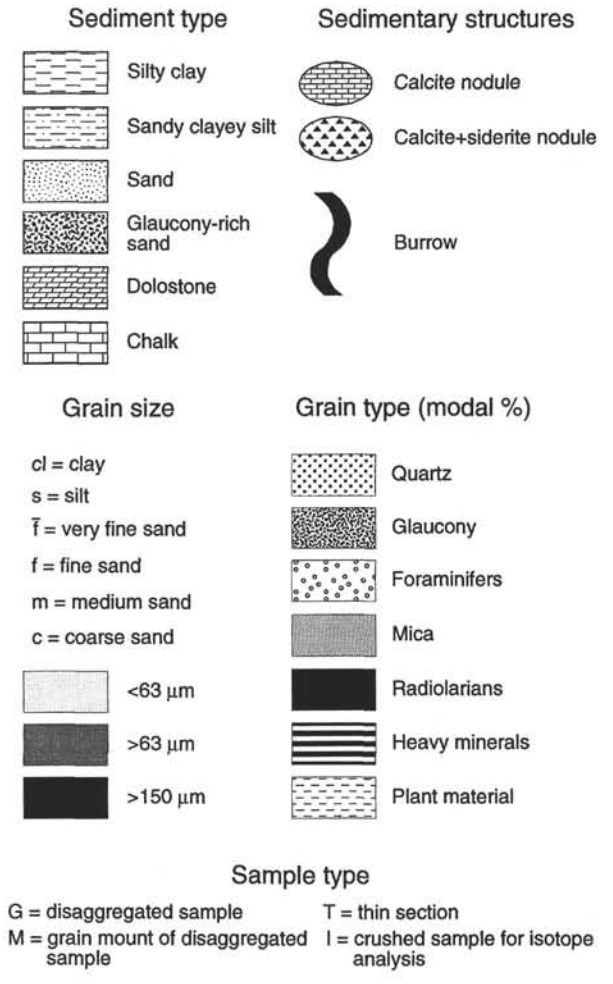

Figure 5. Key for Figures 4, 6, 7, 8, 9, and 10.

requires exposure to seawater on a hiatus surface for 10^5 to 10^6 yr (Fig. 11).

Glaucony: Transported vs. In Situ

The criteria described in the literature to determine the degree of transport undergone by glaucony grains are difficult to apply to samples from Site 903. Glaucony is generally believed to be easily rounded during transport; therefore, well-rounded grains are typically identified as transported grains. This characteristic is not suitable where the substrate replaced by glaucony is itself rounded, such as radiolarians and spherical foraminifers (e.g., *Orbulina*) and as mentioned above, highly evolved grains are characterized by a rounded appearance. Fischer (1990) suggested that the best visual criterion for differentiating between authigenic and detrital glaucony grains is the "presence of well-developed cracks on the grain surface." This criterion is reasonably valid because cracked grains typical of evolved to highly evolved grains would be expected to be highly susceptible to breakage during transport. However, the expansional growth of glaucony grains and possibly bioturbation of the sediment will also result in breakage of evolved to highly evolved grains. Therefore, an in situ, mature population of glaucony would contain a combination of broken grains and complete grains with cracked margins. Other visual criteria for identifying reworked glaucony grains would be the presence of diagenetic alteration features such as pyrite replacement and oxidation as indicated by brownish or reddish glaucony grains. The presence of pyrite, however, is not a reliable criterion when dealing with buried glaucony, because in situ, authigenic glaucony may be pyritized when buried in the sulfate reduction zone. Color is also an unreliable characteristic when dealing with glaucony formed or deposited on the slope. Fluctuations in the position of the oxygen-minimum zone may result in the oxidization of glaucony-forming environment and the subsequent color alteration of the glaucony grains.

The features used in this study to distinguish transported from in situ glaucony are as follows: (1) variability: the presence in a unit of the complete glaucony spectrum from nascent to highly evolved suggests an in situ population of grains; (2) shape and grain size: similarity of the glaucony grains to the grains they replaced indicates that limited reworking and breakage has occurred; and (3) color: brownish and yellowish coloration is suggestive of reworking, whereas in situ grains are typically dark green. It is recognized that these features are not rigorous due to the reasons discussed above, and, where possible, interpretation of the transported vs. in situ nature of the glaucony analyzed for this study is supplemented with independent sedimentological information.

Glaucony at Site 903

The petrography of the glaucony studied from Site 903 define two distinct populations using the criteria discussed above. In situ glaucony characterizes intervals G1 and G2 and reworked glaucony characterizes intervals G3, G4, G5, and G6.

In Situ Glaucony

The glaucony grains observed in intervals G1 and G2 are characteristic of nascent to highly evolved glaucony grains (Fig. 11). The grains display all stages of glauconitization as defined by Odin and Fullagar (1988), ranging from radiolarians partially infilled by pale green glaucony, to pale to dark green grains with partially preserved radiolarian textures, to dark green grains with well-developed surface cracks, to smooth grains resulting from the infilling of surface cracks by light green glaucony (Pl. 1, Figs. 1, 2, 4, and 5). The intermixing of fragmented glaucony grains with evolved and highly evolved grains is consistent with the breakage of grains during the formation of evolved grains (Odin and Fullagar, 1988). The glaucony in intervals G1 and G2 is associated with abundant unaltered radiolarians, and little quartz is present in these intervals. No older, reworked microfossils have been reported from these intervals (Shipboard Scientific Party, 1994). The glaucony of G1 and G2 is interpreted to represent in situ or locally reworked glaucony formed during long hiatuses. The unconformity at the base of the glaucony-rich unit in interval G1 represents a 2- to 6-m.y. (NP19/20 to NP23) break in sedimentation (Shipboard Scientific Party, 1994). Strontium isotopic analysis of foraminifers above and below the glaucony-rich unit in interval G2 suggests a 2-m.y. gap across the erosional surface at the base of the glaucony-rich unit (Miller et al., this volume). Although these time gaps may in part record removal of sediment by erosion, the surfaces at the base of both of these glaucony-rich intervals represent significant breaks in sedimentation. The time gaps represented by these unconformities exceed the minimum time (10^5 to 10^6 yr) required for the formation of highly evolved glaucony grains (Odin and Dodson, 1982).

Reworked Glaucony

The sand-sized glaucony grains in the graded beds of G6 are variably rounded, well sorted, and a brownish-green color (Pl. 3, Fig. 3), whereas the glaucony grains present in the carbonate-cemented clasts in G6 and in intervals G3, G4, and G5 are poorly sorted, are broken, commonly have cracked margins, and are a yellowish-green color (Pl. 3, Figs. 1, 2, and 4). These characteristics suggest that the glaucony of the carbonate-cemented clasts of G6 and of intervals G3, G4, and G5 has undergone less reworking than the glaucony in the graded beds of G6. The similarity of the glaucony within the G6 clasts to the

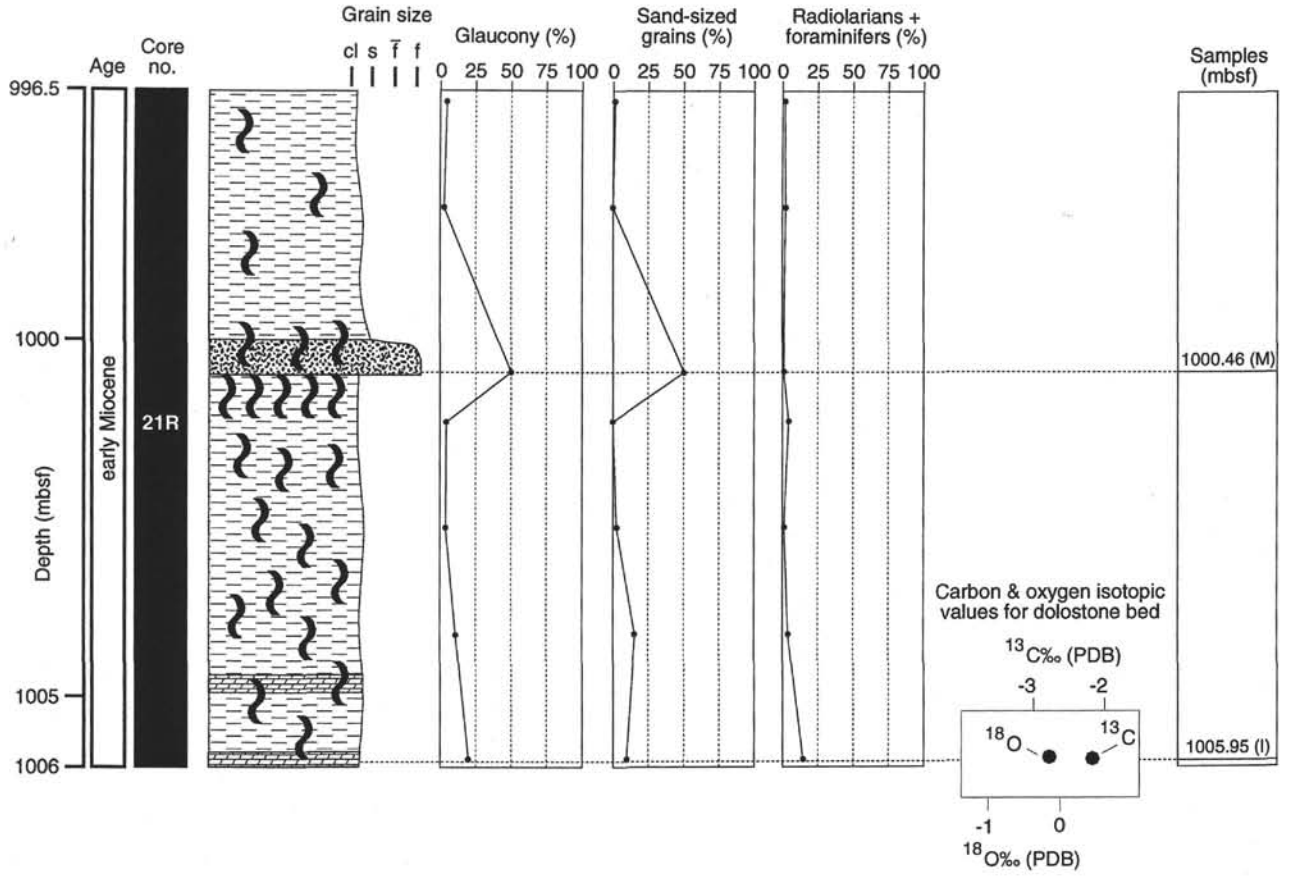

Figure 6. Detailed sedimentological log of glaucony-rich interval G2 (refer to Table 1 for core details). Smear-slide data from Shipboard Scientific Party (1994). See Table 3 for isotopic data. See Figure 5 for the key to symbols used.

glaucony observed in the Miocene intervals G3, G4, and G5, and the presence of possible Miocene foraminifers in these clasts suggest that the clasts were reworked from Miocene strata upslope from Site 903. The p6 sequence boundary, which forms the base of the G6 glaucony-rich interval, can be observed in seismic profiles to truncate upper Miocene strata to the west of Site 903. The general characteristics of the glaucony of the middle to late Miocene section in Site 903 indicate that it has undergone minor reworking and modification, consistent with formation on the shelf and redeposition by turbidity currents on the slope.

Diagenesis of the Glaucony-Rich Intervals

The petrology of the dolomitized zones of G1 and G2 (Pl. 1, Fig. 6, and Pl. 2, Figs. 1 and 2) and their close spatial association with unconformities (Figs. 4, 6) suggest precipitation in the sulfate-reduction zone (Hicks et al., this volume). However, the $\delta^{13}C$ values of these dolomites of about –2‰ (Table 3; Figs. 4, 6) are at odds with this interpretation and are more suggestive of precipitation in the zone of methanogenesis (Hicks et al., this volume). A possible explanation for this contradictory evidence is that the samples analyzed for isotopic composition were a mix of biogenic carbonate, iron-poor dolomite formed in the sulfate-reduction zone, and iron-rich dolomite precipitated in the methanogenesis zone. The observation of dolomite overgrowth on pyrite and zonation of the dolomite from Fe poor to Fe rich is consistent with early pyrite and Fe-poor dolomite precipitation in the sulfate-reduction zone, followed by Fe-rich dolomite precipitation in the methanogenesis zone.

The calcite-siderite nodule present 60 cm below the lower boundary of the glaucony-rich sands in interval G3 has a $\delta^{13}C$ value (Table 3; Fig. 7) suggestive of precipitation in the zone of methanogenesis (Claypool and Kaplan, 1974). There is no independent evidence to indicate the timing of the formation of this nodule relative to the overlying glaucony-rich interval. However, if the precipitation of nodule is assumed to be synchronous with formation of the erosional surface at the base of interval G3, this indicates a condensed diagenetic profile with methanogenesis occurring close to the sediment/water interface. The well-cemented calcite nodules directly below the lower contacts of the glaucony-rich sands in intervals G4 and G5 have $\delta^{13}C$ values (Table 3; Figs. 8, 9) in the range expected for precipitation in the sulfate-reduction zone (Irwin et al., 1977). The presence of diagenetic carbonate nodules below these erosional boundaries indicates that sufficient time was available for carbonate cementation to occur during times of slow or nondeposition (Ellis et al., 1994).

The calcite-cemented nodules present in the graded beds of interval G6 are typical of calcite nodules formed during early burial. The calcite that cements the nodules and infills the shrinkage cracks (Pl. 2, Figs. 5 and 6; Pl. 3, Fig. 4) is iron poor and has negative $\delta^{13}C$ values (Table 3; Fig. 10), which are indicative of precipitation in the sulfate-reduction zone (Irwin et al., 1977; Hicks et al., this volume). However, the presence of possible Miocene foraminifers in these nodules and the strontium isotope age of 16.59 Ma (Hicks et al., this volume) indicate that these nodules did not form in şitu but were reworked from Miocene strata present upslope from Site 903. No diagenetic nodules or beds are present below the lower contact of the glaucony-rich interval in G6.

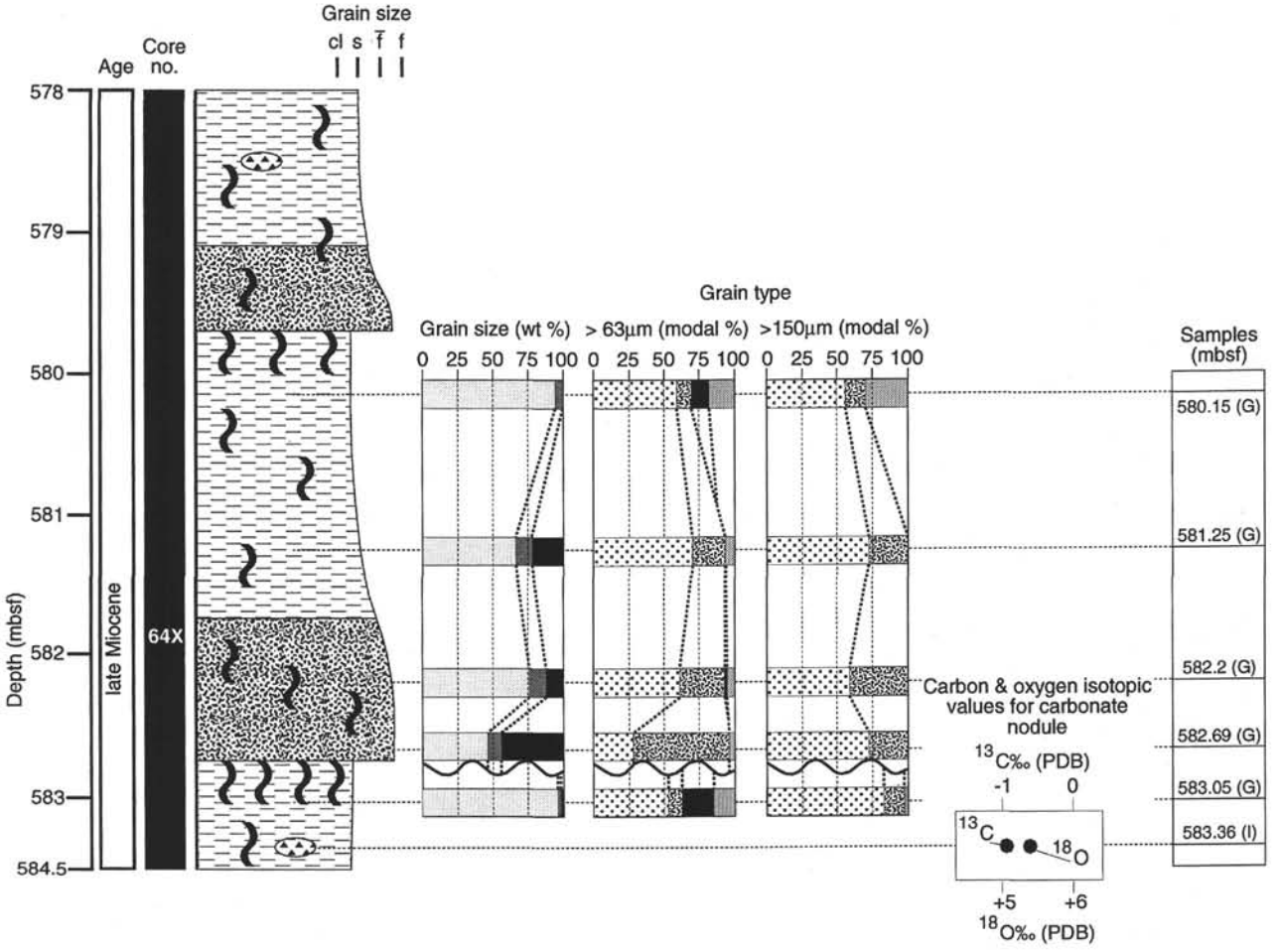

Figure 7. Detailed sedimentological log of glaucony-rich interval G3 (refer to Table 1 for core details). See Tables 2 and 3 for grain size, modal percentage, and isotopic data. See Figure 5 for the key to symbols used.

Sequence-Stratigraphic Significance of Glaucony and Associated Unconformities

The sequence-stratigraphic architecture of slope settings on passive margins, such as that drilled at Site 903, has been largely ignored to date. The majority of discussions are restricted to the zone between the highstand shoreline and the base of the lowstand fan (e.g., Van Wagoner et al., 1988). Haq (1991) discussed the expression of sequences in the deep sea, recognizing that the deep-sea equivalents of shelfal sequence boundaries are typically conformable boundaries. He also recognized that unconformities in the deep sea are in many cases indicative of sediment starvation during maximum flooding of the shelf or ramp. As might be expected, the sequence stratigraphic architecture of the slope is a combination of features observed on the shelf and features observed in the deep sea. Cousin and Thein (1987) described unconformities developed on the midslope of the New Jersey Margin. These unconformities represent large time gaps, and in the Tertiary, are overlain by coarse terrigenous material. These unconformities were correlated (Poag and Ward, 1987) with global unconformities associated with second-order eustatic falls. Unconformities, such as those described by Haq (1991) from the deep sea, associated with sediment starvation, and formed by a combination of bioturbation and erosion caused by deep-sea currents, would also be expected to form on the slope. Therefore, the identification of the mechanisms by which an unconformity forms on the slope clearly has important implications to the development of sequence-stratigraphic models for this setting.

Intervals G1 and G2

Glaucony-rich intervals G1 and G2 are interpreted as slope equivalents of shelfal transgressive system tracts. The age breaks at the base of the glaucony-rich sediment, the highly evolved, nontransported nature of the glaucony, the abundance of radiolarians, the rarity of terrigenous material, and the presence of dolomite-cemented zones below the lower boundaries are features characteristic of intervals of extremely low detrital sedimentation (Loutit et al., 1988). The thick intervals of diatom-rich siltstone and claystone with common silt-sized glaucony above the glaucony-rich intervals in the upper Oligocene–lower Miocene section at Site 903 (Fig. 2; Shipboard Scientific Party, 1994) are a mix of pelagic sedimentation and distal sedimentation during lowstand and highstand. No significant depositional breaks were observed in these mud-rich intervals. As suggested by Haq (1991), sedimentation in a distal setting like Site 903 takes the form of stacked, condensed sequences with no expression of the coeval sequence boundaries observed on the shelf.

Intervals G3, G4, and G5

Interpretation of the glaucony-rich intervals G3, G4, and G5 in a sequence-stratigraphic context is inhibited by the inability to determine confidently whether the glaucony in these intervals was reworked from glaucony-rich sediments contemporaneously deposited on the shelf or reworked from older Eocene to Oligocene strata. The petrological characteristics of the glaucony and the association of

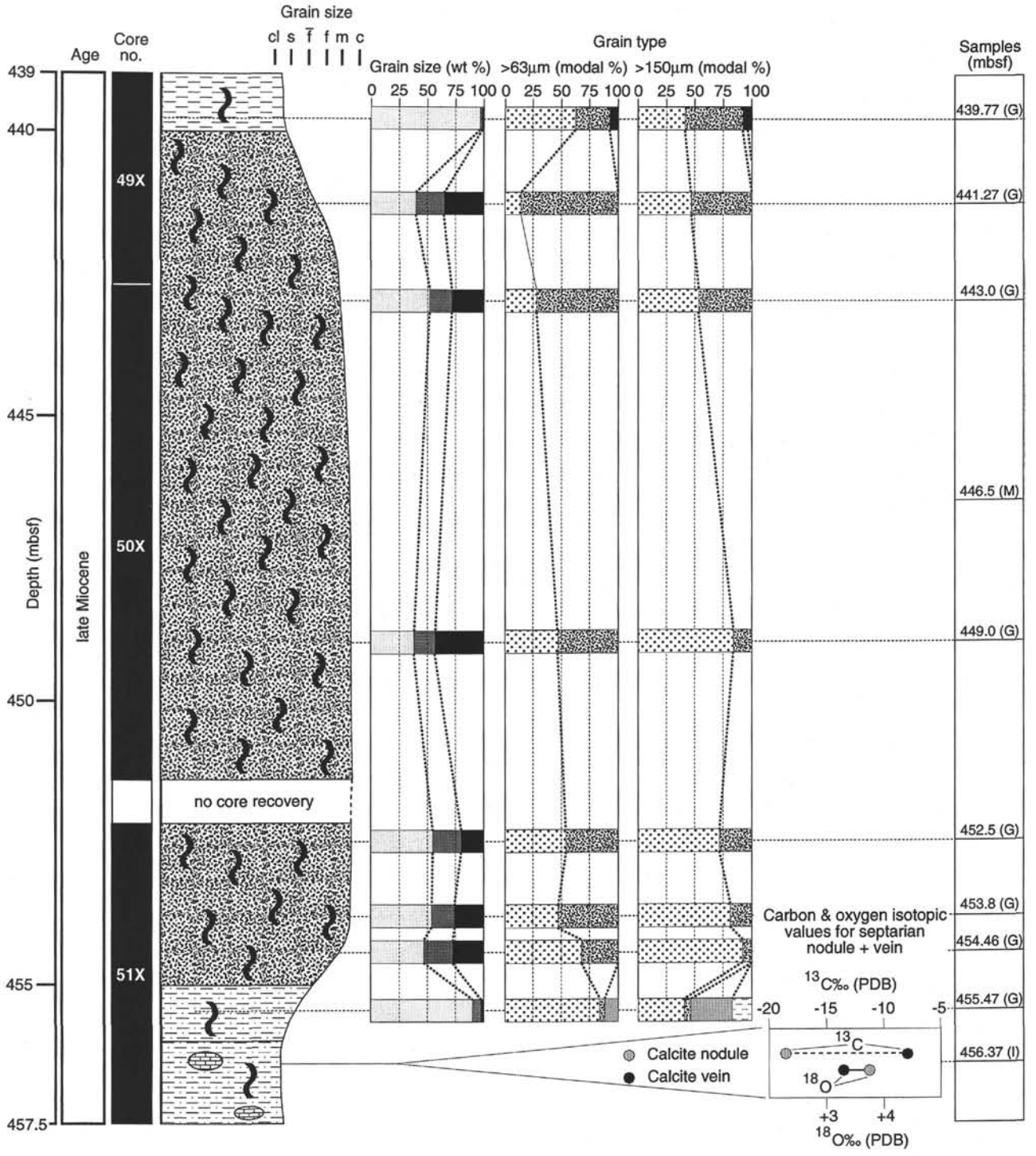

Figure 8. Detailed sedimentological log of glaucony-rich interval G4 (refer to Table 1 for core details). See Tables 2 and 3 for grain size, modal percentage, and isotopic data. See Figure 5 for the key to symbols used.

possible Miocene foraminifers with similar glaucony in the clasts of G6 suggest that this glaucony has undergone only minor reworking and is of Miocene age. Therefore, following the reasoning of Haq (1991) and assuming that the glaucony is reworked, contemporaneously formed, authigenic material, the bioturbated and erosional unconformities would be interpreted to be equivalent to the transgressive system tract on the shelf. The glaucony and quartz-rich sand turbidites would be the result of shedding of transgressive system tract material during early highstand. Preliminary sequence-stratigraphic interpretation of the middle to late Miocene glaucony-rich and quartz-rich units (Fig. 12) is based on these assumptions. In this interpretation, the major type-1 sequence boundaries m1.5, m1, m0.5, m0.3, and p6 that are recognized as downlap or truncation surfaces on seismic profiles (Fig. 2) are overlain by mass-flow deposits dominated by terrigenous sand, typically with abundant plant material. Interpretation of minor sequence boundaries, such as those interpreted to be present at 440.3 and 475.5 mbsf (Fig. 12), is based on minor changes in sediment type. As would be expected with minor sequence boundaries observed on the slope, there is no clear break in sedimentation between the lowstand system tract and the highstand

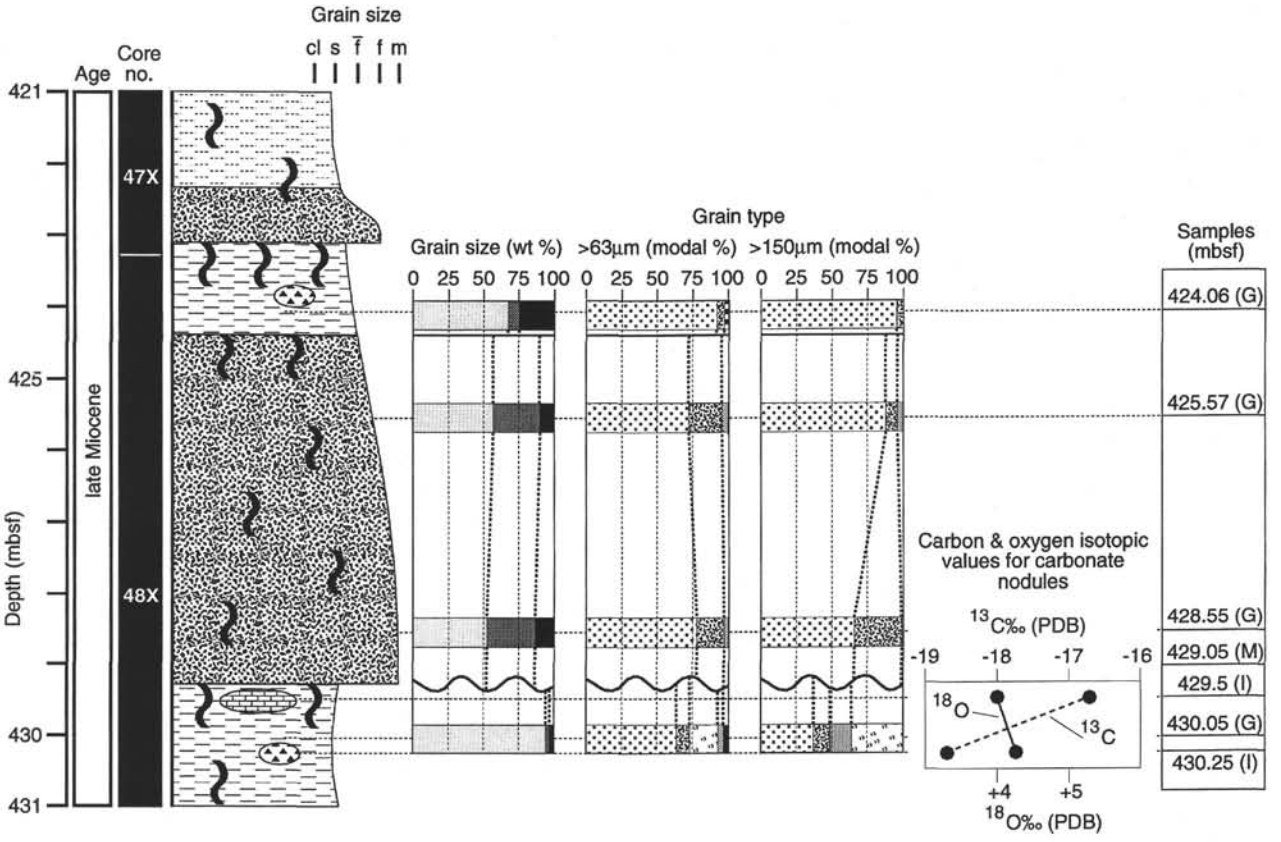

Figure 9. Detailed sedimentological log of glaucony-rich interval G5 (refer to Table 1 for core details). See Tables 2 and 3 for grain size, modal percentage, and isotopic data. See Figure 5 for the key to symbols used.

system tract. Flooding in the middle to upper Miocene section at Site 903 is characterized by the development of bioturbated, erosional surfaces, commonly underlain by carbonate nodules formed during early burial in the sulfate-reduction and methanogenesis zones. These bioturbated, erosional surfaces are the slope equivalent of the transgressive system tract developed on the shelf. These surfaces are typically overlain by glaucony- and quartz-rich sediment interpreted to have been redeposited on the slope during early highstand. Seismic-stratigraphic interpretation of clinoformal packages present updip from Site 903 on Line 1005 suggests the presence of four sequences between seismic reflectors m1 and m0.3, in agreement with the lithologically based interpretation. More information regarding grain-size and grain-type variation and the age of the glaucony is required to provide a more rigorous sequence-stratigraphic interpretation for this section.

Interval G6

The unconformity at the base of the glaucony-rich unit in interval G6 is characteristic of a sequence boundary developed on the slope. It represents a significant break in time, is overlain by coarse clastic material reworked from underlying strata, and can be observed in seismic profiles to be a major truncation surface. There is no evidence of a hiatus associated with this unconformity. This unconformity is similar to erosional surfaces interpreted by Poag and Ward (1987) to be related to second-order sea-level falls.

Oligocene to Miocene Upwelling on the New Jersey Margin

A feature of the New Jersey Margin is the abrupt change from a carbonate ramp in the Eocene to a starved siliciclastic margin in the Oligocene (Greenlee et al., 1992; Miller et al., this volume). This "siliciclastic" switch (Miller et al., this volume) has been attributed to a global cooling (Miller et al., 1991) and is well illustrated at Site 903. The upper Eocene strata at Site 903 consists of nannofossil- and foraminifer-rich, clayey chalk with <1 wt% total organic carbon (TOC) (Shipboard Scientific Party, 1994). In contrast, the upper Oligocene–lower Miocene strata, which unconformably overlie the Eocene chalk, consist of diatom- and nannofossil-rich, glauconitic clayey siltstone with >2 wt% TOC (Shipboard Scientific Party, 1994) with common glaucony-rich layers, such as intervals G1 and G2. This change from a carbonate-rich depositional environment to a silica-rich depositional environment and the marked increase in the preservation of organic matter is consistent with a significant increase in upwelling of cooler, more nutrient-rich water at this time. The Oligocene global cooling resulted in vigorous oceanic circulation (Pickering et al., 1989) and, in turn, increased upwelling. Upwelling of cool, nutrient-rich waters onto the slope and outer shelf is expected to result in increased productivity and a well-developed oxygen-minimum zone (Jenkyns, 1986). The common silt-sized glaucony and moderate sulfur levels (1.5 to 3.5 wt%) present in the upper Oligocene–lower Miocene clayey siltstones at Site 903 (Shipboard Scientific Party, 1994) are consistent with sedimentation within the reducing environment of an oxygen-minimum zone.

CONCLUSIONS

Detailed investigation of six glaucony-rich units of late Oligocene, early to late Miocene, and middle Pliocene–early Pleistocene age recovered at Site 903 indicates that the presence of glaucony in sediment deposited on the continental slope is not always an indicator of condensed sedimentation. Three characteristics are critical in the

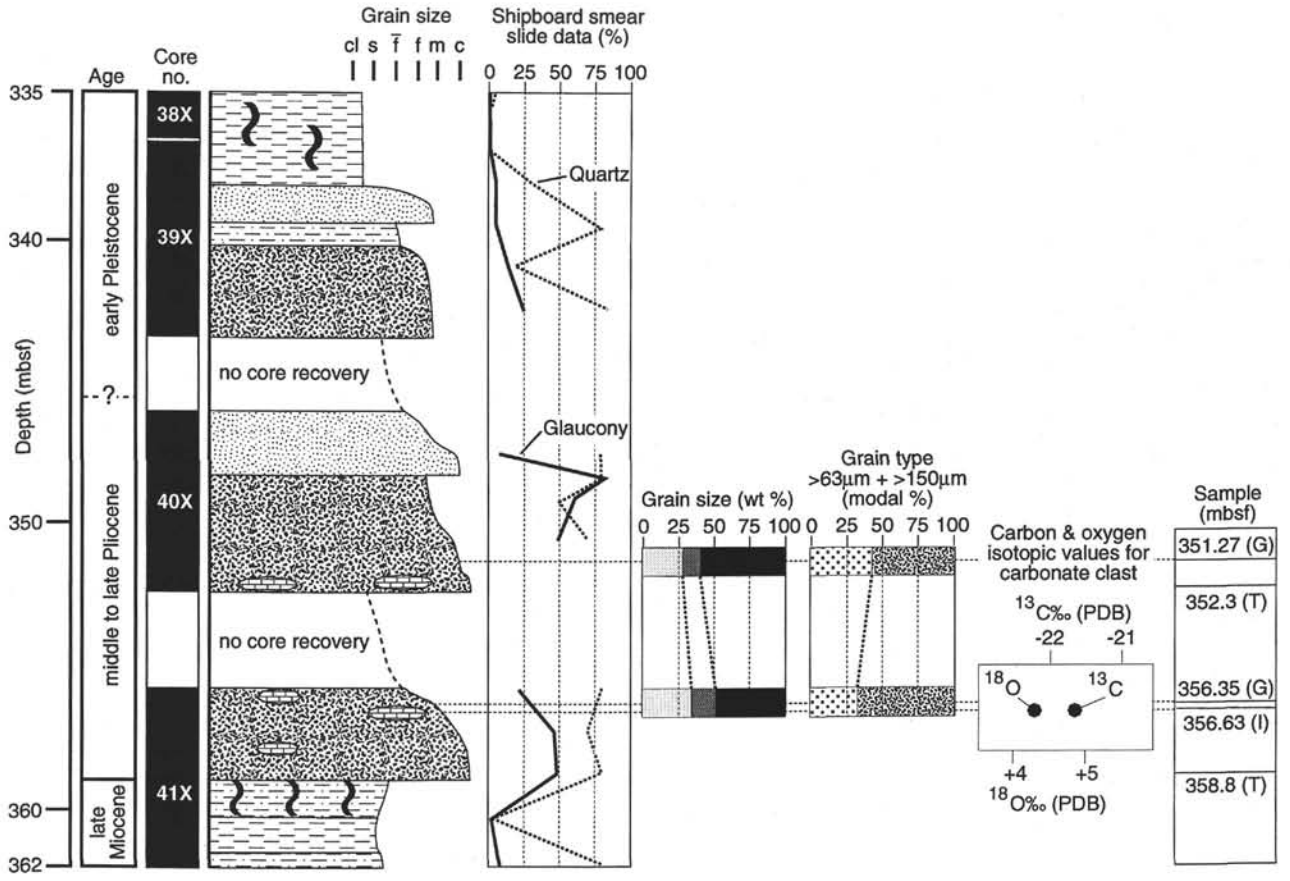

Figure 10. Detailed sedimentological log of glaucony-rich interval G6 (refer to Table 1 for core details). Smear-slide data from Shipboard Scientific Party (1994). See Tables 2 and 3 for grain size, modal percentage, and isotopic data. See Figure 5 for the key to symbols used.

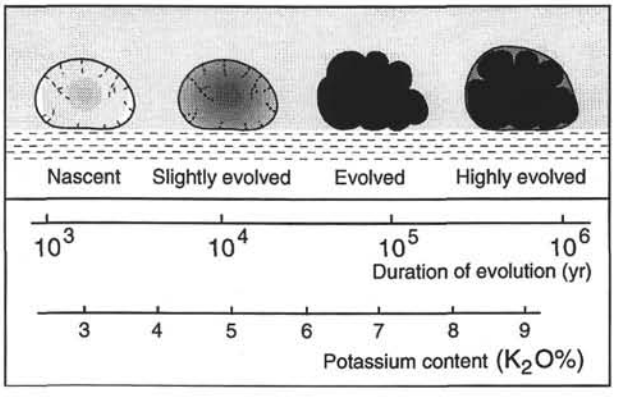

Figure 11. Stages of glauconitization of a granular substrate (after Odin and Dodson, 1982).

sequence-stratigraphic interpretation of glaucony-rich sediment on the slope: (1) the degree of reworking of the glaucony prior to final deposition; (2) the relative abundances of terrigenous and biogenic material in the glaucony-rich unit; and (3) the sedimentological and diagenetic characteristics of the lower boundary of the glaucony-rich unit. These features are vital in distinguishing among glaucony formed in situ, reworked from coeval, shelfal environments, and reworked from older, glaucony-bearing strata.

The glaucony-rich sediments observed at Site 903 were deposited at three different stages within the depositional sequence. The upper Oligocene to lower Miocene glaucony-rich units (G1 and G2) overlie erosional unconformities that represent significant age gaps and are characterized by highly evolved, authigenic glaucony associated with abundant radiolarians. These glaucony-rich units were deposited during flooding of the shelf and represent condensed sections. The middle to upper Miocene glaucony-rich units investigated for this study (G3, G4, and G5) overlie bioturbated, erosional surfaces underlain by carbonate nodules. These surfaces are the result of sediment starvation during flooding of the shelf. The glaucony-rich sediment that overlies the surfaces was redeposited from condensed sections of the transgressive system tract during early highstand. Minor glaucony is also present in the late highstand and lowstand sediments associated with these units. The middle Pliocene–lower Pleistocene glaucony-rich sediment (G6) overlies a major truncation surface (sequence boundary) and was deposited during a lowstand of sea level and associated erosion of the shelf and upper slope.

ACKNOWLEDGMENTS

We thank the members of the Leg 150 scientific party, Ocean Drilling Program staff, the SEDCO crew, Mike Power for stable isotopic analyses of the carbonate samples, Malcolm Wallace for assistance with the cathodoluminescence microscope, Russel Perembo for identification of foraminifers in thin sections, and Richard Howe for assistance with the plates. Critical reviews by Annette George, Patrick Coleman, Stephen Hesselbo, Greg Mountain, and Paul Fullagar and an anonymous reviewer greatly improved the style and content of the manuscript.

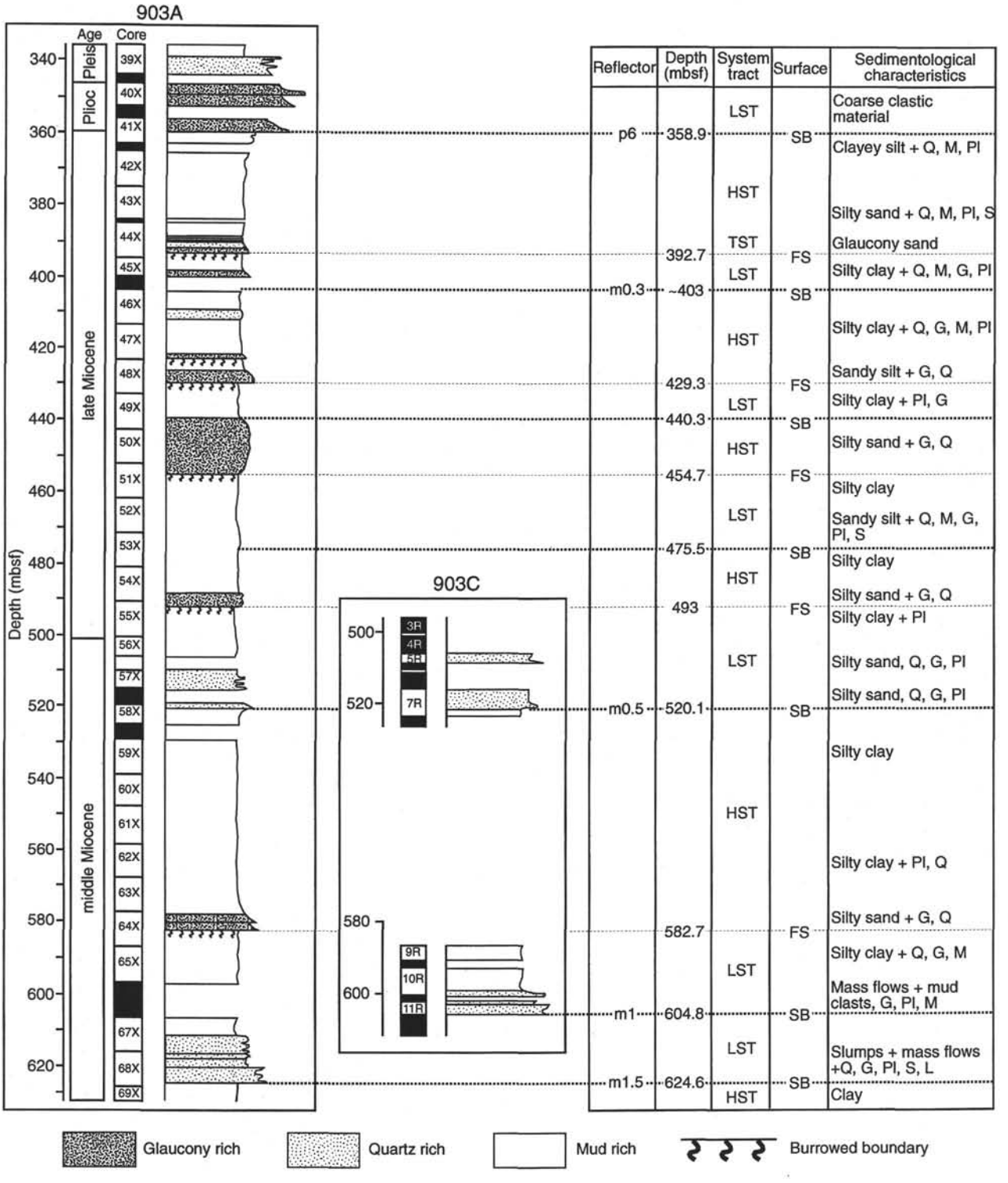

Figure 12. Sequence-stratigraphic interpretation of the middle to upper Miocene section drilled at Site 903. LST = lowstand system tract, HST = highstand system tract, TST = transgressive system tract, SB = sequence boundary, FS = flooding surface, Q = quartz, G = glaucony, M = mica, Pl = plant material, S = shell fragments, L = lithic clasts.

REFERENCES

Claypool, G.E., and Kaplan, I.R., 1974. The origin and distribution of methane in marine sediments. *In* Kaplan, I.R. (Ed.), *Natural Gases in Marine Sediments:* New York (Plenum), 99–139.

Cousin, M., and Thein, J., 1987. Lithologic and geochemical changes across unconformities at Site 612, Deep Sea Drilling Project Leg 95, New Jersey Transect. *In* Poag, C.W., Watts, A.B., et al., *Init. Repts. DSDP,* 95: Washington (U.S. Govt. Printing Office), 549–564.

Craig, H., 1957. Isotopic standards for carbon and oxygen and correction factors for mass-spectrometric analysis of carbon dioxide. *Geochim. Cosmochim. Acta,* 12:133–149.

Ellis, G., Tait, A.M., and Gibson, P.J., 1994. Mid-Cretaceous concretionary carbonate reservoirs at Barrow Island, Western Australia. *In* Purcell, P.G., and Purcell, R.R. (Eds.), *The Sedimentary Basin of Western Australia: Proceedings of the Petroleum Exploration Society of Australia Symposium,* 459–475.

Fischer, H., 1990. Glauconite formation: discussion of the terms authigenic, perigenic, allogenic, and meta-allogenic. *Eclogae Geol. Helv.,* 83:1–6.

Greenlee, S.M., Devlin, W.J., Miller, K.G., Mountain, G.S., and Flemings, P.B., 1992. Integrated sequence stratigraphy of Neogene deposits, New Jersey continental shelf and slope: comparison with the Exxon model. *Geol. Soc. Am. Bull.,* 104:1403–1411.

Greenlee, S.M., and Moore, T.C., 1988. Recognition and interpretation of depositional sequences and calculation of sea level changes from stratigraphic data-offshore New Jersey and Alabama Tertiary. *In* Wilgus, C.K., Posamentier, H., Ross, C.A., and Kendall, C.G.St.C. (Eds.), *Sea-level Changes: An Integrated Approach.* Spec. Publ.—Soc. Econ. Paleontol. Mineral., 42:329–353.

Haq, B.U., 1991. Sequence stratigraphy, sea-level change, and significance for the deep sea. *In* Macdonald, D.I.M. (Ed.), *Sedimentation, Tectonics and Eustasy: Sea Level Changes at Active Margins.* Spec. Publ. Int. Assoc. Sedimentol., 12:3–39.

Hower, J., 1961. Some factors concerning the nature and origin of glauconite. *Am. Mineral.,* 46:313–334.

Irwin, H., Curtis, C.D., and Coleman, M.L., 1977. Isotopic evidence for the source of diagenetic carbonates formed during burial of organic-rich sediments. *Nature,* 269:209–213.

Jenkyns, H.C., 1986. Pelagic environments. *In* Reading, H.G. (Ed.), *Sedimentary Environments and Facies* (2nd ed.): Oxford (Blackwell Sci.), 343–397.

Loutit, T.S., Hardenbol, J., Vail, P.R. and Baum, G.R., 1988. Condensed sections: the key to age determination and correlation of continental margin sequences. *In* Wilgus, C.K., Hastings, B.S., Ross, C.A., Posamentier, H.W., Van Wagoner, J., and Kendall, C.G.St.C. (Eds.), *Sea-Level Changes: An Integrated Approach.* Spec. Publ.—Soc. Econ. Paleontol. Mineral., 42:183–213.

McCrea, T., 1950. The isotopic chemistry of carbonates and a paleotemperature scale. *J. Chem. Phys.,* 18:849–857.

Miller, K.G., and Mountain, G.S., 1994. Global sea-level change and the New Jersey margin. *In* Mountain, G.S., Miller, K.G., Blum, P., et al., *Proc. ODP, Init. Repts.,* 150: College Station, TX (Ocean Drilling Program), 11–20.

Miller, K.G., Wright, J.D., and Fairbanks, R.G., 1991. Unlocking the Ice House: Oligocene-Miocene oxygen isotopes, eustasy, and margin erosion. *J. Geophys. Res.,* 96:6829–6848.

Millot, G., 1970. *Geology of Clays:* New York (Springer-Verlag).

Odin, G.S. (Ed.), 1988. *Green Marine Clays:* Amsterdam (Elsevier).

Odin, G.S., and Dodson, M.H., 1982. Zero isotopic age of glauconies. *In* Odin, G.S. (Ed.), *Numerical Dating in Stratigraphy:* Chichester (Wiley), 277–306.

Odin, G.S., and Fullagar, P.D., 1988. Geological significance of the glauconies facies. *In* Odin, G.S. (Ed.), *Green Marine Clays:* Amsterdam (Elsevier), Dev. in Sedimentol. Ser., 45:295–332.

Odin, G.S., and Matter, A., 1981. Die glauconarium origine. *Sedimentology,* 28:611–643.

Pickering, K.T., Hiscott, R., and Hein, F.J., 1989. *Deep-marine Environments: Clastic Sedimentation and Tectonics:* London (Unwin Hyman).

Poag, C.W., and Ward, L.W., 1987. Cenozoic unconformities and depositional supersequences of the North Atlantic continental margins: testing the Vail model. *Geology,* 15:159–162.

Shipboard Scientific Party, 1994. Site 903. *In* Mountain, G.S., Miller, K.G., Blum, P., et al., *Proc. ODP, Init. Repts.,* 150: College Station, TX (Ocean Drilling Program), 129–205.

Stille, P., and Clauer, N., 1994. The process of glauconitization: chemical and isotopic evidence. *Contrib. Mineral. Petrol.,* 117:253–262.

Vail, P.R., Mitchum, R.M., Jr., Todd, R.G., Widmier, J.M., Thompson, S., III, Sangree, J.B., Bubb, J.N., and Hatlelid, W.G., 1977. Seismic stratigraphy and global changes in sea level. *In* Payton, C.E. (Ed.), *Seismic Stratigraphy: Applications to Hydrocarbon Exploration.* AAPG Mem., 26:49–212.

Van Wagoner, J.C., Posamentier, H.W., Mitchum, R.M., Jr., Vail, P.R., Sarg, J.F., Loutit, T.S., and Hardenbol, J., 1988. An overview of the fundamentals of sequence stratigraphy and key definitions. *In* Wilgus, C.K., Hastings, B.S., Ross, C.A., Posamentier, H.W., Van Wagoner, J., and Kendall, C.G.St.C. (Eds.), *Sea-Level Changes: An Integrated Approach.* Spec. Publ.—Soc. Econ. Paleontol. Mineral., 42:39–45.

Date of initial receipt: 9 March 1995
Date of acceptance: 17 October 1995
Ms 150SR-015

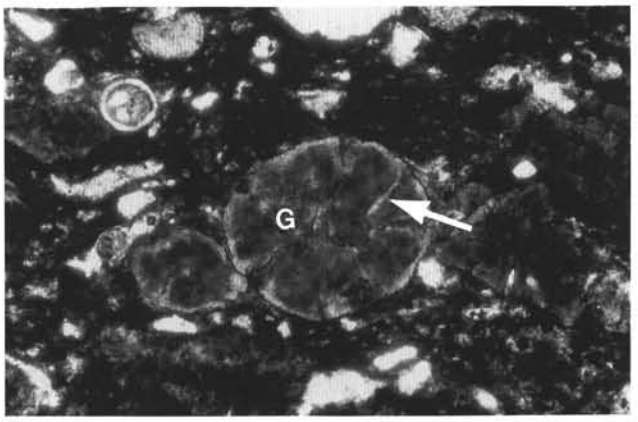

1

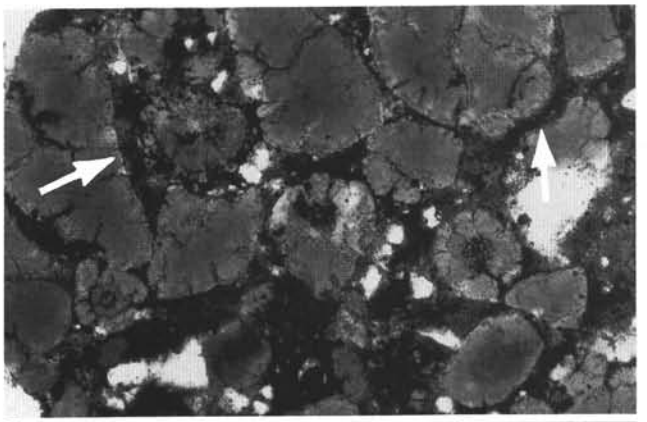

2

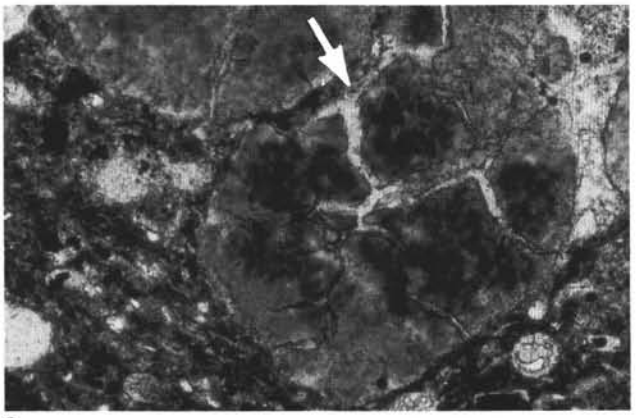

3

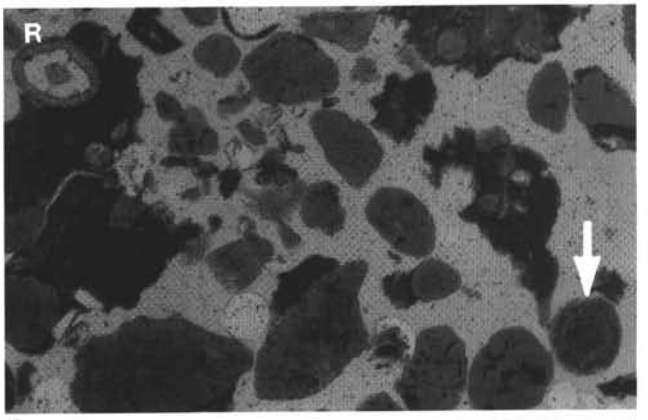

4

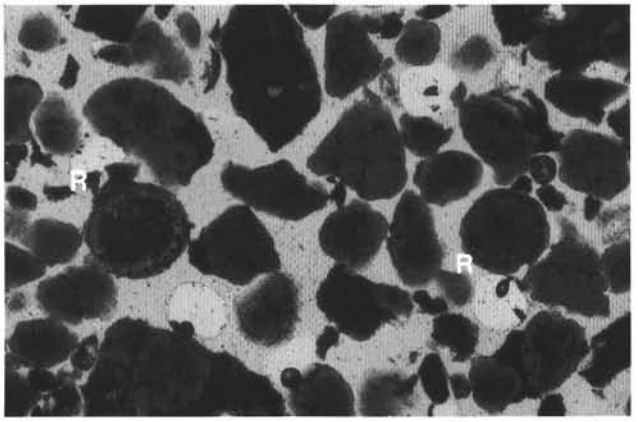

5

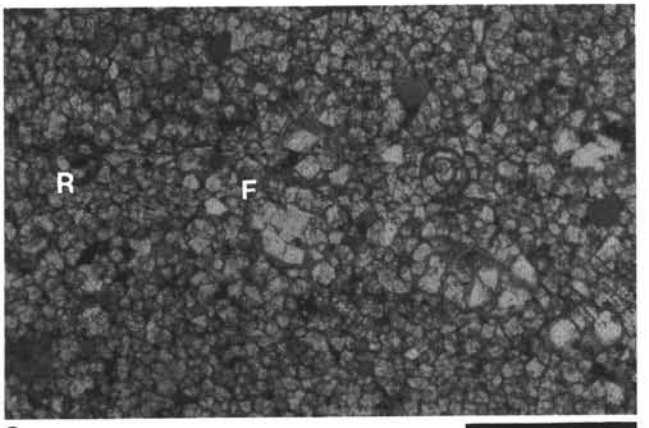

6

Plate 1. **1.** Sample 150-903C-51R-6, 147–149 cm. Highly evolved grain (G). Note lighter glaucony rimming the darker, cracked grain (arrow) (scale bar = 0.5 mm). **2.** Sample 150-903C-51R-7, 90–92 cm. Evolved and highly evolved grains of glaucony. Note the presence of pyritized radiolarians (arrows) within the highly evolved grains and cracked and pyritized margins of the grains (scale bar = 1 mm). **3.** Sample 150-903C-51R-7, 120–122 cm. Silica cement-infilling of compaction-related fractures (arrow) formed at grain/grain contact. Compaction layering in matrix cemented by calcite and silica cements (scale bar = 0.5 mm). **4.** Sample 150-903D-21R-4, 100–102 cm. "Evolved" and "highly evolved" grains and angular to poorly rounded fragments of glaucony. Note presence of non-glauconized (R) and totally glauconized radiolarians (arrow) (scale bar = 1 mm). Thin section of grain mount. **5.** Same sample as Figure 4. Evolved and highly evolved grains and angular to poorly rounded fragments of glaucony. Note the presence of radiolarians (R) within the highly evolved grains (scale bar = 1 mm). **6.** Sample 150-903D-21R-8, 49–52 cm. Dolomitized radiolarian- (R) and foraminifer- (F) rich silt clay (scale bar = 1 mm).

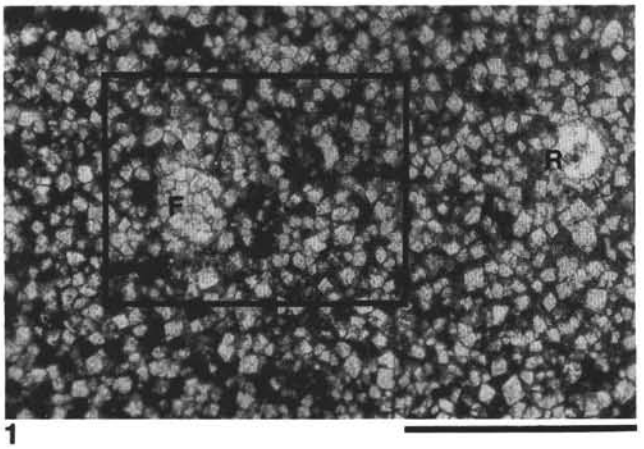

1

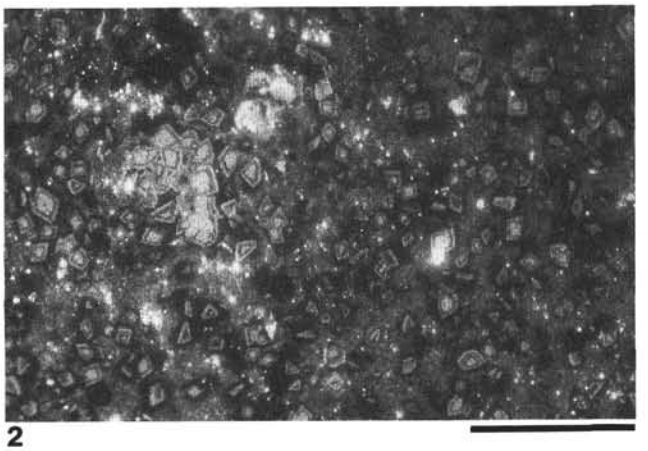

2

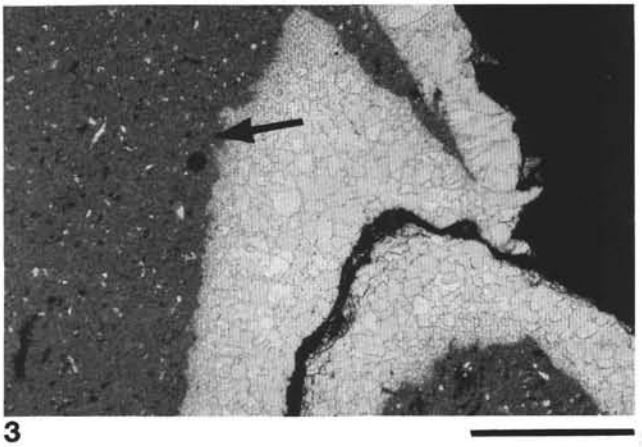

3

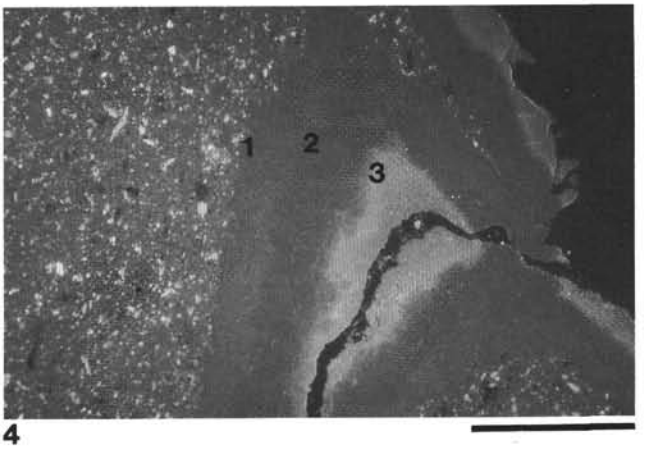

4

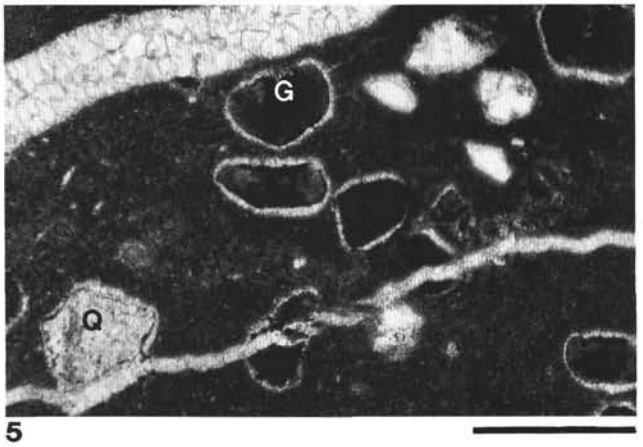

5

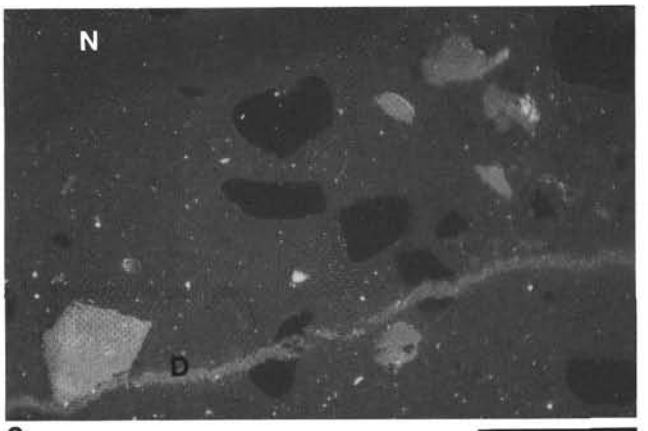

6

Plate 2. **1.** Sample 150-903C-52R-1, 15–17 cm. Dolomitized chalk. Note infilling of foraminifer (F) and radiolarian (R) tests with dolomite (scale bar = 0.5 mm). **2.** Cathodoluminescent micrograph of area marked on Figure 1. Note the multiple zones within a single dolomite rhomb (scale bar = 0.25 cm). **3.** Sample 150-903A-51X-3, 116–118 cm. Calcite-lined septarian vein within a calcitic micrite nodule. Note framboidal pyrite in the body of the nodule (arrow) (scale bar = 1 mm). **4.** Cathodoluminescent micrograph of same field of view as Figure 3. Note three different phases of calcite (1, 2, and 3) based on luminescent character (scale bar = 1 mm). **5.** Sample 150-903A-41X-1, 89–94 cm. Medium sand-sized quartz (Q) and glaucony (G) in a calcite-cemented nodule. Note the shrinkage cracks around grains (arrow) and crosscutting fractures related to shrinkage of the nodule, both infilled with calcite (scale bar = 0.5 mm). **6.** Cathodoluminescent micrograph of same field of view as Figure 5. Calcite infilling large vein and cracks around the grains is nonluminescent (N), and the calcite infilling the thin vein that crosscuts the calcite around the grains has a dull orange luminescence (D) (scale bar = 0.5 mm).

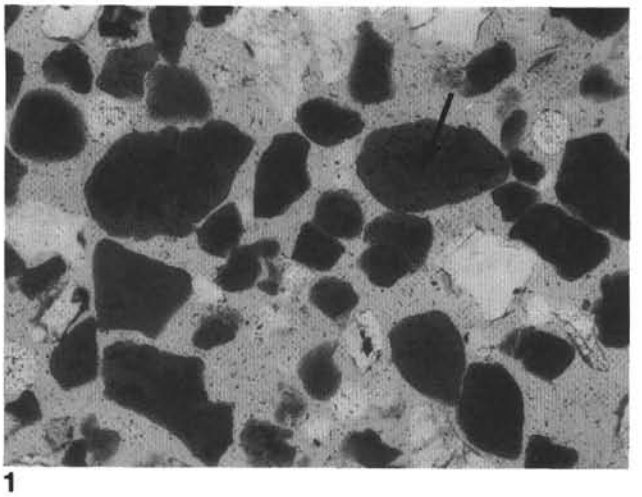

1

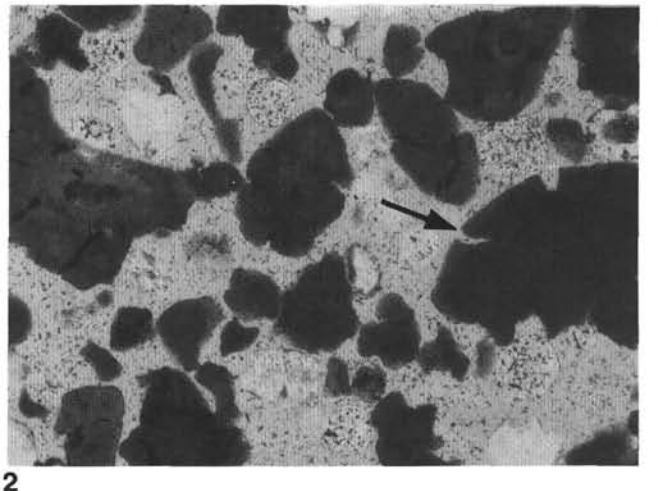

2

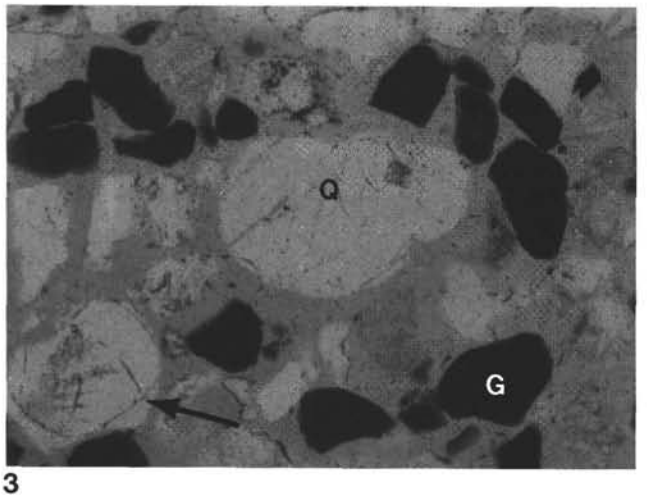

3

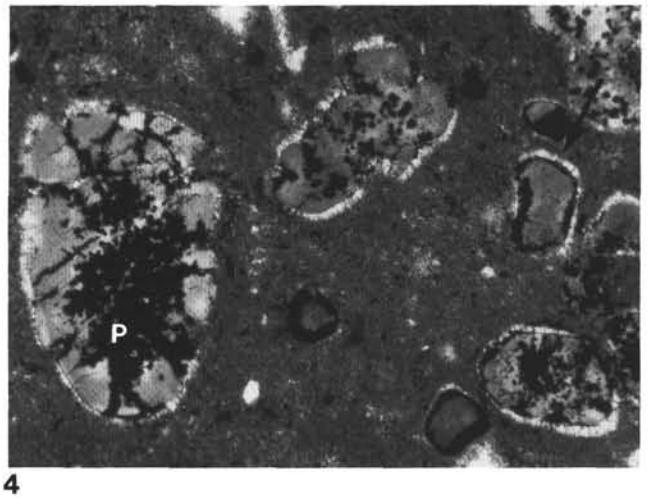

4

Plate 3. **1.** Sample 150-903A-50X-3, 80–82 cm. Medium to coarse sand-sized, yellowish-green glaucony and quartz. Rare glaucony grains have cracked margins (arrow) (scale bar = 1 mm). Thin section of grain mount. **2.** Sample 150-903A-48X-4, 125–127 cm. Fine to coarse sand-sized, dark yellowish-green glaucony. Note cracked margins of some fragmented glaucony grains (arrow) (scale bar = 1 mm). Thin section of grain mount. **3.** Sample 150-903A-41X-1, 10–12 cm. Medium to coarse quartz sand grains (Q) with quartz overgrowths (arrow) and fine sand grains of poorly to moderately well-rounded, dark green-brown glaucony (G) (scale bar = 1 mm). Thin section of grain mount. **4.** Sample 150-903A-41X-1, 89–94 cm. Medium sand-size glaucony grains in a calcite-cemented nodule. Pyrite (P) has replaced the cores of the glaucony grains and partially rimmed the grains. Calcite infilling of the shrinkage cracks around the grains postdates pyritization (arrow) (scale bar = 1 mm).